Research Square

Preprints are preliminary reports that have not undergone peer review.
They should not be considered conclusive, used to inform clinical practice,
or referenced by the media as validated information.

A chimeric oncolytic poxvirus overcomes barriers to systemic cancer virotherapy

Philippe Erbs

erbs@transgene.fr

Transgene https://orcid.org/0000-0002-6810-4610

Johann Foloppe

Transgene

Annie Findeli

Transgene

Jules Deforges

Transgene

Isabelle Farine

Transgene

Christelle Pichon

Transgene

Juliette Kempf

Transgene

Michele Klein

Transgene

Julie Hortelano

Transgene

Baptiste Moreau

Transgene

Sandrine Cochin

Transgene

Benoit Grellier

Transgene

Article

Keywords: Oncolytic virotherapy, Directed evolution, Systemic delivery, Immune evasion

Posted Date: September 2nd, 2026

DOI: https://doi.org/10.21203/rs.3.rs-10348774/v1

License: This work is licensed under a Creative Commons Attribution 4.0 International License.
Read Full License

Additional Declarations:
There is **NO** Competing Interest.

Human serum samples were obtained from patients enrolled in the clinical study NCT03724071. The study was approved by the Comité de Protection des Personnes Est IV (HUS, Hôpital Civil, Strasbourg, France), the Comité d'Éthique de l'Institut Jules Bordet (Brussels, Belgium), and the Comité de Ética de la Investigación con Medicamentos (CEIm) HM Hospitales (Madrid, Spain). All participants provided written informed consent prior to enrollment and study participation.

A chimeric oncolytic poxvirus overcomes barriers to systemic cancer virotherapy

Johann Foloppe, Annie Findeli, Jules Deforges, Isabelle Farine, Christelle Pichon, Juliette Kempf, Michele Klein, Julie Hortelano, Baptiste Moreau, Sandrine Cochin, Benoit Grellier, Philippe Erbs*

Affiliations: Transgene, Illkirch-Graffenstaden, France

*To whom correspondence should be addressed: erbs@transgene.fr

Abstract

Systemic delivery remains a major challenge in oncolytic virotherapy due to rapid immune neutralization, limited tumor dissemination, and insufficient induction of antitumor immunity. Here, we describe PoxSTG, a next-generation chimeric oncolytic poxvirus generated through stringent directed evolution across multiple orthopoxvirus species, yielding a mosaic virus with non-parental properties. PoxSTG exhibits enhanced replication and cytolytic activity in human tumor cells while remaining attenuated in normal tissues. It combines extensive syncytial fusion with increased extracellular enveloped virus production, promoting efficient intratumoral spread and systemic propagation. PoxSTG resists complement- and antibody-mediated neutralization and retains infectivity in the presence of humoral immunity. The virus induces caspase-3/GSDME-dependent pyroptosis, enhancing immunogenic cell death. In vivo, PoxSTG displays potent antitumor activity and preferentially expands tumor-specific T-cell responses without augmenting antiviral immunity. IL-12 arming further improves therapeutic efficacy, supporting PoxSTG as a platform for systemic oncolytic virotherapy.

Keywords

Oncolytic virotherapy, Directed evolution, Systemic delivery, Immune evasion

Introduction

Oncolytic viruses (OVs) are an increasingly prominent class of cancer immunotherapeutics capable of selectively lysing malignant cells, enhancing antitumor immune responses, and reshaping the tumor microenvironment[1]. Their development includes neoadjuvant applications and combinations with chemotherapy, immune checkpoint inhibitors, CAR T cell therapies, and other immunomodulatory agents[2-6]. Despite these advantages, clinical responses have remained modest, and only a few OVs—notably talimogene laherparepvec (T-VEC)—have received regulatory approval[7]. Factors contributing to this translational gap include the immunocompromised status of many patients and dosing regimens insufficient to induce durable immune activation[8]. Encouragingly, interim Phase 3 data for the adenoviral OV CG0070 in non–muscle invasive bladder cancer reported a 75% complete response rate with sustained activity, underscoring the therapeutic potential of OVs when efficiently delivered[9]. Together with T-VEC, these findings highlight the importance of effective local delivery. However, intratumoral administration is not feasible for many solid tumors, making systemic delivery an attractive alternative. Intravenous administration, however, faces major challenges: rapid neutralization by antibodies and complement, dilution in circulation, sequestration by endothelial and reticuloendothelial systems, and inefficient tumor spread. Addressing these barriers is critical for advancing systemically deliverable OVs[10, 11]. Vaccinia virus (VACV), a member of the poxvirus family historically used in the eradication of smallpox[12], represents a promising oncolytic virus (OV) backbone owing to its rapid lytic cycle, well-established safety profile, and large genomic capacity[13]. Genetic modifications can enhance tumor selectivity and immunogenicity[14]. We previously developed TG6002, an attenuated oncolytic VACV carrying deletions in thymidine kinase (J2R) and ribonucleotide reductase (I4L) to promote tumor-selective replication and expressing the FCU1 prodrug-converting enzyme, which converts non-toxic 5-fluorocytosine (5-FC) into 5-fluorouracil (5-FU)[15, 16]. An open-label phase I dose-escalation trial of intravenous TG6002 plus oral 5-FC in advanced gastrointestinal cancers (NCT03724071) showed good tolerability with no maximum tolerated dose, effective tumor biodistribution, and localized FCU1 activity[17]. A separate study using hepatic artery delivery (NCT04194034) in liver-dominant metastatic colorectal cancer confirmed safety and demonstrated targeted tumor delivery, viral replication, FCU1 expression, immune activation,

and early signs of antitumor activity[18]. However, both intravenous and intrahepatic administration resulted in rapid induction of neutralizing antibodies, even at low doses[17, 18], a finding also reported in canine models following intratumoral injection[19]. The emergence of neutralizing immunity therefore represents a major limitation for systemic VACV-based therapies and highlights the need for more potent viral platforms capable of maintaining antitumor activity despite humoral barriers. While many OVs under clinical evaluation derive from naturally occurring viral strains, these viruses did not evolve to act as cancer therapeutics; their tumor tropism reflects incidental features of viral biology. Directed evolution offers a complementary approach to rational engineering by enabling complex, therapeutically relevant traits to emerge under defined selective pressure[20]. We previously used such a strategy by pooling four VACV strains, yielding a recombinant virus with enhanced oncolytic properties. Iterative selection led to the isolation of deVV5, a chimeric variant with improved tumor cell killing and increased selectivity in vitro[21].

In the current study, we expanded our directed evolution framework by incorporating a broader and more diverse panel of parental poxviruses and by applying more stringent selection conditions. This strategy generated PoxSTG, a tumor-tropic chimeric orthopoxvirus backbone. We show that PoxSTG integrates multiple advantageous features: enhanced replication and cytolysis in human tumor cells, reduced replication in normal tissues, improved dissemination through combined syncytial fusion and extracellular enveloped virus (EEV) production, resistance to complement and antibody-mediated neutralization, and the ability to induce immunogenic, pyroptotic cell death. These properties translate into robust antitumor activity and preferential induction of tumor-specific immunity. Together, our findings establish PoxSTG as a next-generation platform designed to overcome the key limitations of systemic OV therapy.

Results

Directed evolution generates a human-optimized chimeric virus

A direct evolution strategy was employed to generate chimeric poxviruses with enhanced oncolytic potency and tumor selectivity. A diverse viral library was first established by co-infecting A549 cells with 16 distinct poxvirus strains (Fig. 1A). The A549 cell line, known for its high permissiveness to viral infection, facilitated extensive recombination among co-infecting viruses, thereby increasing the diversity of resulting chimeric clones. To enrich viruses with superior oncolytic properties, consecutive passages were performed under stringent selection conditions, including high dilution (1:10,000) and short harvest times (24 hours post-infection), favoring the emergence of fast-replicating and highly cytolytic variants. From passage 9, forty-eight individual plaque-purified clones were isolated. One clone, exhibiting superior cytolytic activity on A549 cells, was further screened for oncolytic potency across a panel of tumor cell lines (Fig. 1B). This clone, designated PoxSTG, demonstrated markedly enhanced oncolytic activity on human tumor cell lines compared to the parental VACV Copenhagen strain (COP), previously identified as the most effective reference strain [21, 22]. In contrast, no gain of activity was observed in murine tumor lines, indicating species-selective optimization toward human cells.

A mosaic orthopoxvirus genome with preserved architecture

Genomic DNA from PoxSTG and its 16 parental virus species or strains was purified and sequenced using Next Generation Sequencing (NGS). The lengths of the assembled genomes, including PoxSTG, are listed in Supplementary Table 1. Comparative analysis of the de novo assemblies revealed that PoxSTG is a recombinant mosaic derived from six poxviruses: Rabbitpox virus (RPXV), Cowpox virus (CPXV), and the VACV strains Wyeth (WY), Western Reserve (WR), Copenhagen (COP), and Modified Vaccinia Ankara (MVA) (Fig. 1C). Nearly all genomic segments map identically to parental sequences, consistent with homologous recombination. Despite this mosaic structure, genome organization and ORF positioning are preserved (Supplementary Table 2). Phylogenetically, PoxSTG clusters within the vaccinia clade while remaining genetically distinct (Fig. 1D).

Enhanced tumor selectivity and transgene performance

To improve the therapeutic profile of PoxSTG, the viral thymidine kinase (J2R/TK) locus was deleted and replaced with the GFP::FCU1 fusion gene, generating PoxSTG19508. TK deletion

did not compromise oncolytic activity; instead, PoxSTG19508 retained the superior cytolytic efficacy of PoxSTG and consistently outperformed all TK-deleted parental orthopoxvirus strains across A549, HCT116 and Hep G2 tumor cell lines (Fig. 2A). These findings indicate that virus chimerization generates a backbone with enhanced oncolytic potential. For the remainder of the study, most comparisons were made against the VACV strain Copenhagen (COP), which is currently under clinical evaluation and has demonstrated superior oncolytic activity in preclinical models compared to other orthopoxviruses[21, 22]

Functional expression of FCU1 was confirmed by measuring conversion of 5-FC into 5-FU in infected A549 cells. Compared with the FCU1-expressing VACV control CopTG17111, PoxSTG19508 mediated substantially higher 5-FC conversion, reaching >40% and >90% at days 2 and 3 post-infection, respectively, versus 15% and 60% for CopTG17111 (Fig. 2B). This enhanced prodrug activation likely reflects the increased replication capacity of the chimeric virus in tumor cells.

Tumor selectivity was assessed in primary human hepatocytes and a reconstituted human skin model. Relative to vaccinia Copenhagen (COP), PoxSTG showed reduced replication in normal tissues while replicating more efficiently in Hep G2 tumor cells (Fig. 2C), resulting in an improved tumor specificity index (Fig. 2D). Importantly, TK deletion further decreased replication in normal cells by approximately eightfold, while preserving robust replication in tumor cells, thereby markedly increasing the tumor-to-normal cell replication ratio (Fig. 2C,D). Together, these data demonstrate that PoxSTG19508 combines enhanced oncolytic potency, superior FCU1-mediated prodrug activation, and improved tumor selectivity.

Synergistic dissemination via fusion and extracellular spread

To investigate mechanisms underlying the superior oncolytic activity of PoxSTG, cell-to-cell fusion was evaluated in HCT116 cells infected with either CopTG17111 or PoxSTG19508. Whereas CopTG17111 infection induced the typical rounded-cell phenotype without membrane fusion, PoxSTG19508 triggered progressive syncytium formation, resulting in large multinucleated cell structures with diffuse GFP distribution throughout the fused cytoplasm (Fig. 3A). We next quantified production of intracellular mature virus (IMV) and extracellular enveloped virus (EEV) in infected A549 cells. Although total viral yields were only ~2-fold higher for PoxSTG19508 than for CopTG17111, EEV production was markedly enhanced, with 20–40-fold higher EEV titers detected at 16 and 24 h post-infection (Fig. 3B). Consequently, the EEV/IMV ratio increased from ~0.5% for CopTG17111 to >5% and >10% for PoxSTG19508 at 16 and 24 h, respectively (Fig. 3C), indicating more efficient early release of

extracellular virions. Consistent with these findings, PoxSTG19508 formed characteristic comet-shaped plaques under liquid-overlay conditions, a hallmark of efficient EEV-mediated viral spread, whereas CopTG17111 generated only compact plaques typical of the vaccinia Copenhagen strain (Fig. 3D). Together, these results show that PoxSTG19508 promotes syncytium formation and markedly enhances extracellular virus dissemination, two features likely contributing to its improved oncolytic activity.

Induction of pyroptotic tumor cell death

To determine whether PoxSTG induces pyroptosis, tumor cells were analyzed for morphological and molecular hallmarks of inflammatory cell death. Compared with CopTG17111, PoxSTG infection induced pronounced cell swelling, membrane blebbing, and bubble-like protrusions characteristic of pyroptosis (Fig. 4A). Consistent with loss of membrane integrity, PoxSTG triggered significantly greater release of lactate dehydrogenase (LDH), IL-18, and DAMPs, including High Mobility Group Box 1 (HMGB1) and adenosine triphosphate (ATP) (Fig. 4B–E). At the molecular level, PoxSTG activated the caspase-3/GSDME pathway, as evidenced by cleavage of pro-caspase-3 (~32 kDa) into its active fragments (~17–19 kDa) and generation of the pore-forming N-terminal gasdermin E (GSDME) fragment (~30–35 kDa) at 48 h post-infection (Fig. 4F,G). Together, these findings demonstrate that PoxSTG induces pyroptotic tumor cell death through activation of the caspase-3/GSDME axis, leading to membrane rupture and release of inflammatory mediators. These effects were markedly reduced or absent in cells infected with the parental viruses, indicating a qualitative shift in cell death modality.

Resistance to complement and antibody neutralization

PoxSTG19508 exhibited marked resistance to complement-mediated neutralization, retaining 86% of its infectivity after incubation with normal human serum, whereas CopTG17111 titers were reduced to ~1% of control levels (Fig. 5A). Resistance to antibody-mediated neutralization was evaluated using sera from a TG6002-treated patient and a PoxSTG-treated dog. In both cases, CopTG17111 was efficiently neutralized, resulting in a pronounced increase in EC_{50} values (Fig. 5B,D,E,G). In contrast, PoxSTG19508 largely maintained its cytotoxic activity in the presence of immune sera, showing no significant neutralization by patient serum and only modest neutralization by dog serum (Fig. 5C,D,F,G). These findings demonstrate that PoxSTG19508 partially evades both complement- and antibody-mediated antiviral responses, a property that may enhance viral persistence and therapeutic efficacy.

Improved antitumor efficacy in vivo

The antitumor activity of PoxSTG19508 was compared with that of CopTG17111 in xenograft and syngeneic mouse models. Following a single intravenous administration at suboptimal doses of CopTG17111, PoxSTG19508 produced substantially greater tumor growth inhibition than CopTG17111 in both HCT116 and Hep G2 xenografts (Fig. 6A,C). Complete tumor regression was achieved in 66.6% versus 22.2% of HCT116-bearing mice and in 40% versus 0% of Hep G2-bearing mice treated with PoxSTG19508 and CopTG17111, respectively. These responses translated into significantly prolonged survival (Fig. 6B,D). In the CT26 syngeneic model, three high-dose intratumoral injections of PoxSTG19508 induced complete tumor regression in 40% of mice, compared with 20% for CopTG17111, and significantly prolonged survival (Fig. 7A,B). Interestingly, this enhanced in vivo efficacy occurred despite similar in vitro activity of the two viruses against murine tumor cells (Fig. 1B), suggesting that factors beyond direct tumor cell killing contribute to the superior therapeutic effect of PoxSTG19508. To evaluate the therapeutic potential of transgene arming, a double TK/RR-deleted chimeric virus expressing murine IL-12 (PoxSTG19847) was generated and compared with its vaccinia Copenhagen counterpart (CopTG19328). In the aggressive B16F10 syngeneic melanoma model, intravenous administration of PoxSTG19847 markedly delayed tumor growth and significantly prolonged survival relative to CopTG19328 (Fig. 7C,D). Together, these findings demonstrate the superior therapeutic efficacy of the chimeric virus platform across diverse tumor models and support its further development as a transgene delivery backbone.

Preferential tumor-specific immune activation

To compare antiviral and antitumor immunity elicited by treatment, splenocytes from CT26 tumor-bearing mice treated with PBS, CopTG17111, or PoxSTG19508 were stimulated ex vivo with either the tumor-associated AH1 peptide, the vaccinia-specific S9L8 peptide, or an irrelevant peptide. PoxSTG19508 induced a significantly stronger AH1-specific T cell response than CopTG17111, whereas vaccinia-specific T cell responses were comparable between the two viruses (Fig. 7E). These results indicate that the chimeric virus preferentially enhances tumor-specific immunity without increasing antiviral immune responses.

Enhanced intratumoral and systemic dissemination

The intratumoral dissemination of PoxSTG19508 was compared with that of CopTG17111 in xenograft and syngeneic tumor models. Following intravenous administration in HCT116 xenografts, both viruses initially infected comparable tumor areas (~2% at day 2). However,

whereas CopTG17111 subsequently spread to only 10–20% of the tumor area, PoxSTG19508 disseminated extensively, occupying >50% of the tumor mass within 1–2 weeks (Fig. 8A,B). Similarly, in B16F10 tumors and following intratumoral administration, vaccinia antigen was transient and barely detectable after CopTG17111 treatment, whereas strong and persistent staining was observed following PoxSTG19508 administration, indicating enhanced spread in murine tumors (Fig. 8C,D). To assess systemic dissemination, mice bearing bilateral HCT116 xenografts received a single intratumoral injection into one tumor only. Although both viruses controlled growth at the injected site, PoxSTG19508 achieved a higher rate of complete regressions than CopTG17111 (40% versus 10%; Fig. 8E). Strikingly, only PoxSTG19508 induced regression of distant, untreated tumors, with complete responses observed in 30% of non-injected lesions (Fig. 8F), resulting in a significant survival benefit (Fig. 8G). Consistent with these findings, viral titration demonstrated efficient replication of both viruses in injected tumors, whereas PoxSTG19508, but not CopTG17111, was detected in contralateral tumors (Fig. 8H). Together, these results demonstrate that PoxSTG19508 exhibits superior intratumoral and systemic dissemination, enabling effective targeting of distant tumor sites.

Discussion

Using a directed-evolution strategy across multiple orthopoxvirus species, we generated the chimeric backbone PoxSTG and its TK-deleted, transgene-armed derivative PoxSTG19508. These viruses combine several properties desirable for next-generation oncolytic virotherapy, including enhanced replication and cytotoxicity in human tumor cells, increased tumor selectivity, efficient intratumoral and systemic dissemination, resistance to humoral neutralization, potent antitumor activity in vivo, and preferential induction of tumor-specific immunity. Together, these features distinguish PoxSTG from conventional VACV backbones and support its development as a platform for systemic cancer therapy. The selection strategy imposed an unusually stringent evolutionary pressure. Sixteen orthopoxvirus strains were co-infected into human tumor cells and serially passaged under conditions in which only cell-free supernatants harvested at 24 h were transferred. This selection strategy, which was more stringent than previously reported approaches[21, 23], inherently favored viruses capable of rapid replication, efficient progeny production, and early dissemination. Whole-genome sequencing revealed that PoxSTG is a mosaic virus composed of genomic segments derived from several orthopoxvirus species, including rabbitpox, cowpox, vaccinia, and MVA. Such recombination likely enabled the assembly of favorable allelic combinations that collectively enhance viral fitness in human tumor cells while preserving the overall genomic organization characteristic of orthopoxviruses. Functionally, PoxSTG displayed large gains in human cancer cell lines but only modest gains in murine cells, indicating that key determinants acquired during selection act through human-biased pathways (e.g., host-range factors controlling translation, antiviral antagonists, or immune-evasion genes with species-restricted activity). Notably, PoxSTG replication was reduced in primary non-transformed cells—an advantageous safety feature. Deletion of J2R (TK)—a classical safety lever that attenuates VACV in quiescent primary cells while sparing rapidly dividing tumor cells[24]—further reduced replication in human primary skin and hepatocytes yet preserved amplification in cancer cells, increasing the tumor-to-normal ratio. Insertion of the FCU1::GFP transgene into the TK locus provided an additional therapeutic mechanism through local conversion of 5-FC into 5-FU. The greater prodrug conversion achieved by PoxSTG19508 compared with an equivalent vaccinia vector likely reflects enhanced intratumoral replication and transgene expression, highlighting the value of the evolved backbone for therapeutic payload delivery.

A central feature of PoxSTG is its exceptional capacity for viral spread. Compared with vaccinia Copenhagen, PoxSTG induced extensive syncytium formation and produced substantially

higher levels of EEV. These two mechanisms are complementary. Syncytium formation enables direct cell-to-cell transmission without requiring extracellular virion release,[25] while EEV production facilitates long-range dissemination through tumor tissue and vascular compartments[26]. Both properties are likely major contributors to the superior tumor colonization observed in vivo. Genomic analysis provides a plausible mechanistic explanation for the fusogenic phenotype. The PoxSTG genome contains a rabbitpox-derived A56R allele carrying an N-terminal truncation that is predicted to disrupt formation of the fusion-inhibitory A56/K2 complex[27]. Loss of this inhibitory interaction would permit activation of the viral entry-fusion machinery at the surface of infected cells, thereby promoting syncytium formation, direct lateral spread[28, 29] and partial evasion of neutralizing antibodies[30]. Similar fusogenic phenotypes have been associated with enhanced antitumor efficacy in other oncolytic virus platforms[31-33], suggesting that the ability to exploit cell-cell fusion may represent an important determinant of therapeutic activity. In parallel, PoxSTG exhibited a marked increase in EEV production, generating 20–40-fold more EEV than the vaccinia comparator. The presence of the rabbitpox-associated A34R K151E substitution likely contributes to this phenotype, as this mutation is known to promote EEV release and comet plaque formation[34]. The PoxSTG A34R sequence also contains the MVA-derived A19V mutation, suggesting that this locus may have arisen by recombination between Rabbitpox- and MVA-related sequences. Enhanced EEV production provides several potential advantages, including improved virion mobility, greater penetration within solid tumors, and more effective systemic dissemination[35]. Consistent with these properties, PoxSTG spread throughout a substantially larger fraction of tumor tissue following systemic administration and was uniquely capable of establishing productive infection in distant, non-injected tumors. The enhanced EEV phenotype also appears to underlie the remarkable resistance of PoxSTG to humoral neutralization. Unlike IMV, EEV particles possess an additional membrane that masks many of the dominant neutralizing epitopes targeted by antiviral antibodies[36]. Consistent with this biology, PoxSTG19508 retained most of its infectivity after exposure to non–heat-inactivated human serum and proved largely resistant to neutralization by sera obtained from both VACV-treated patients and PoxSTG-treated animals. In contrast, the vaccinia comparator was almost completely neutralized. Partial escape from complement- and antibody-mediated inactivation may be particularly important for systemic administration, where antiviral immunity remains a major limitation for repeated dosing and efficient delivery to disseminated tumors. The phenotypic consequences of enhanced spread and humoral resistance were evident across multiple tumor models. In both HCT116 and Hep G2 xenografts, a single intravenous administration of PoxSTG19508 produced greater tumor

regressions and improved survival than vaccinia Copenhagen. Similar superiority was observed in syngeneic models despite the relatively low permissiveness of murine tumors to poxvirus replication. Most notably, only PoxSTG19508 was capable of efficiently reaching and controlling distant, uninjected tumors following local administration, demonstrating a level of systemic dissemination that is rarely achieved by oncolytic VACVs.

Another important finding of this study is the ability of PoxSTG to induce pyroptotic tumor cell death. Infected tumor cells exhibited hallmark features of pyroptosis, including cellular swelling, membrane blebbing, and robust release of IL-18, HMGB1, ATP, and LDH. Mechanistically, these effects were associated with activation of the caspase-3/GSDME axis and generation of the pore-forming N-terminal fragment of GSDME. Notably, these molecular and phenotypic signatures were largely absent following infection with either parental virus, indicating that the chimeric genome fundamentally alters the mode of tumor cell killing. Pyroptosis has emerged as a highly immunogenic form of programmed cell death that can amplify antitumor immunity through the release of inflammatory cytokines, damage-associated molecular patterns, and tumor antigens, thereby enhancing dendritic-cell activation, antigen presentation, and T-cell priming[37, 38]. Consistent with this concept, PoxSTG elicited stronger tumor-specific T-cell responses than vaccinia Copenhagen while generating comparable antiviral immune responses. This distinction is particularly important because excessive antiviral immunity can accelerate viral clearance and limit the therapeutic window of oncolytic virotherapy[39]. The ability of PoxSTG to preferentially enhance tumor-directed rather than virus-directed immunity suggests that it may act as an effective in situ cancer vaccine while preserving sufficient viral persistence to sustain oncolysis and continuous antigen release. Increasing evidence indicates that induction of pyroptosis contributes to the therapeutic activity of several oncolytic viruses. Coxsackievirus B3, ORF virus, and Zika virus have all been reported to induce GSDME-dependent pyroptotic cell death in tumor cells[40-42]. Furthermore, given that gasdermin family proteins are essential effectors of pyroptosis but are frequently downregulated or epigenetically silenced in human cancers[43], a variety of engineering strategies have been designed to restore or potentiate pyroptotic signaling. For example, engineering oncolytic viruses to express gasdermins, including M1 virus and adenovirus platforms, has been shown to enhance pyroptosis, promote immunogenic cell death, and improve antitumor efficacy[44, 45]. Unlike these approaches, PoxSTG induces robust GSDME-dependent pyroptosis without the need for exogenous gasdermin expression, suggesting that reassortment of the vaccinia, cowpox and rabbitpox genomes intrinsically reprograms virus–host interactions

toward a more inflammatory form of cell death. This property may represent a key mechanistic advantage of the platform, coupling efficient tumor infection with the generation of a highly immunogenic tumor microenvironment.

The versatility of the platform was further illustrated by arming the virus with IL-12. Expression of murine IL-12 from a double-deleted PoxSTG backbone significantly enhanced efficacy in the aggressive B16F10 melanoma model compared with a similarly armed VACV. Because IL-12 promotes NK-cell activation, Th1 polarization, and $CD8^+$ T-cell responses[46], these results suggest that the improved dissemination and persistence of PoxSTG can be leveraged to increase the effectiveness of immunomodulatory payloads. The platform may therefore be broadly applicable for delivery of cytokines, immune engagers, checkpoint inhibitors, or other transgenes designed to remodel the tumor microenvironment.

Several limitations warrant further investigation. Although murine models provide valuable information regarding efficacy and immune activation, the strong preference of PoxSTG for human tumor cells highlights the need for evaluation in more clinically relevant systems, including patient-derived xenografts and humanized mouse models. Long-term genomic stability of the mosaic genome will also require careful assessment during manufacturing and serial passaging. In addition, the combination of enhanced systemic dissemination and partial resistance to humoral neutralization necessitates comprehensive biodistribution, shedding, and environmental safety studies. Finally, the specific genomic elements acquired through reassortment with vaccinia, cowpox, and rabbitpox viruses that confer novel properties, including enhanced tumor selectivity and increased induction of pyroptosis, remain to be elucidated and represent an important focus for future mechanistic studies.

In conclusion, PoxSTG represents a distinct class of evolved oncolytic poxvirus that combines efficient tumor-selective replication, enhanced intratumoral and systemic spread, partial escape from humoral immunity, and potent induction of tumor-focused immune responses. These characteristics provide a strong rationale for further development of the platform, both as a standalone therapeutic and as a delivery vehicle for immunomodulatory payloads. If translated clinically, PoxSTG could help overcome several long-standing barriers to systemic oncolytic virotherapy and provide an effective strategy for the treatment of disseminated malignancies.

Methods

Cell lines and viruses

Human colon cancer cell line HCT116 (CCL-247), human lung cancer cell line A549 (CCL-185), human hepatocarcinoma cell line Hep G2 (HB 8065), human glioblastoma cancer cell line U-87 MG (HTB-14™), human pancreatic cancer cell line PANC-1 (CRL-1469™), human cervical carcinoma cell line HeLa (CCL-2), human ovarian cancer cell line SK-OV-3 (HTB-77), human bladder cancer cell line UM-UC-3 (CRL-1749), murine melanoma cell line B16F10 (CRL-6475), murine colon carcinoma cell line CT26 (CRL-2638) and Vero cell line (CCL-81) were obtained from the American Type Culture Collection (ATCC, Rockville, MD). All cell lines were grown in recommended media supplemented with 10% fetal calf serum (FCS). Fresh human hepatocytes were purchased from Biopredic International (Rennes, France) and maintained in the recommended hepatocyte medium provided by the supplier (Biopredic International). The Phenion full-thickness skin model, a 3D tissue construct that simulates histological and physiological properties of human skin, was purchased from Henkel (Düsseldorf, Germany). This organotypic epithelial raft culture model was maintained in tissue culture medium according to the manufacturer's instructions. Primary chicken embryo fibroblasts (CEF) were used for recombination and production of viral vectors. CEF cells were prepared as previously described [47] and maintained in Eagle-based Medium (MBE) supplemented with 5 % FCS. Wild type VACV Western Reserve strain (WR, ATCC VR-119), wild type VACV Wyeth strain (WY, ATCC VR-1536), wild type Cowpox virus strain Brighton (CPXV, ATCC VR-302), wild type Raccoonpox virus strain Herman (RCNV, ATCC VR-838), wild type Rabbitpox virus strain Utrecht (RPXV, ATCC VR-1591), wild type Bovine Papular Stomatitis virus strain Illinois 721 (BPSV, ATCC VR-801), wild type ORF virus strain NZ2 (ORFV, ATCC VR-1548), wild type Pseudo-cowpox virus strain TJS (PCPV, ATCC VR-634), wild type Myxoma virus strain Lausanne (MYXV, ATCC VR-1829), wild type Yaba-like disease virus strain Davis (YLDV, ATCC VR- 937), wild type Swinepox virus strain Kasza (SWPV, ATCC VR-363), wild type Cotia virus strain SP AN 32 (CTV, ATCC VR-464) and wild type Squirrel Fibroma virus strain Kilham (SQFV, ATCC VR-236) were obtained from ATCC. The wild-type VACV Copenhagen strain (COP) used in this work was previously described [47]. Modified Vaccinia Ankara (MVA) expressing the *GFP* gene under the control of the p11k7.5 promoter (MVA15938) was constructed and characterized previously [48]. Wild type Fowlpox virus strain FP9 (FWPV) was kindly provided by Pr Skinner. The double thymidine

kinase/ribonucleotide reductase (TK/RR)-deleted VACV Copenhagen strain expressing GFP (CopTG17990) or FCU1 (TG6002) was previously constructed and characterized [15, 49]. Single thymidine kinase (TK)-deleted cowpox virus encoding the *GFP::FCU1* fusion gene (CPXTG18831) was previously constructed and characterized [50].

Neutralizing antibody assay

A neutralizing antibody assay was used to determine the titer of VACV neutralizing antibodies (VACV-NAbs) in serum. Two-fold serial dilutions of serum samples were incubated with the GFP expressing VACV CopTG17990 for 1 hour at 37 °C. The diluted serum-virus mixtures were then added to Vero cells for CopTG17990 titration by plaque assay. After three days of incubation, Vero cell culture plates were examined using a fluorescence microscope to score the virus-infected cells (plaque). The neutralizing antibody titer was defined as the highest serum dilution preventing ≥ 50 % plaque formation.

Patient-derived serum fluid

Serum was obtained from patients enrolled in phase 1 clinical trial evaluating the safety and tolerability of multiple-ascending doses of the double TK/RR-deleted Copenhagen strain VACV TG6002 administered intravenously in patients with advanced gastro-intestinal tumors (NCT03724071). All patients gave written informed consent according to good clinical practice guidelines. Serum samples from a patient collected one day before IV administration of TG6002 and 42 days after virus administration were used for VACV/PoxSTG neutralization assay. For the serum collected before TG6002 administration, the VACV-NAb titer was below the limit of detection (<20), while this titer was 4580 for the serum collected 42 days post-infection.

Dog-derived serum fluid

Dog serum was obtained from a healthy adult male Beagle dog following intravenous administration of the double TK/RR-deleted PoxSTG19730 virus. The virus was delivered by intravenous infusion at a dose of 1×10^7 pfu/kg, administered as a repeated schedule on Day 0, Day 2, and Day 4. The study was conducted at BIOVIVO – VetAgro Sup (Veterinary Campus of Lyon, France) in accordance with Biovivo's standard operating procedures and in full compliance with European regulations on animal experimentation (Directive 2010/63/EU). Ethical approval was granted by the VetAgro Sup Ethics Committee (CEEA n°18), and the study was registered under APAFIS#28501-2020102714365353 with the French Ministry of Higher Education and Research. Serum samples collected one day before IV administration of PoxSTG19730 and 21 days after the initial dose were used for VACV/PoxSTG neutralization assay. For the serum collected before PoxSTG administration, the VACV-NAb titer was below

the limit of detection (<20), while this titer was 420 for the serum collected 21 days post-infection.

Directed evolution for selection of Chimeric Poxviruses

Sixteen poxviruses (COP, WY, WR, MVA-GFP, CPXV, RCNV, RPXV, BPSV, ORFV, PCPV, MYXV, YLDV, SWPV, CTV, SQFV, FWPV) were mixed and used to infect the permissive human A549 cells (1.5 x 10^6 cells/well in a 6 well-plate) and constituted the initial virus mix. The mix used for the first passage consisted of 1.5 x 10^4 PFU of each virus corresponding to a Multiplicity of Infection (MOI) of 10^{-2} for each virus. One day post-infection, cells and supernatant from the first initial virus mix were harvested and then used entirely to infect a confluent T-75 tissue culture flask (T75) of A549 cells (passage 1). Cells and supernatant were harvested 72 h post-infection and 1 mL of this mix was used to infect a confluent T75 flask of A549 cells (passage 2). Seventy-two hours post-infection, one mL of cells and supernatant from the second passage was used to infect a T75 flask of A549 cells. Supernatant from the third passage was then used in a 10-fold dilution series to infect a T75 flask of A549 cells. Amplification and selection of viral progeny was done by additional passages (passage 3 to passage 9) on A549 cells by supernatant dilution. The infected T75 were observed for the first signs of cytopathic effect (CPE). From passage 3 to passage 9, to harvest the most potent viruses, cell culture supernatant was harvested 24 H post-infection from the flask infected with the most concentrated inoculum in the 10-fold dilution series that did not show any sign of potent CPE. From passage 9, 48 individual plaque-purified viruses were isolated, amplified, and titrated on A549 cells. Oncolytic activities of these clones were then evaluated on A549 tumor cell line.

DNA sequencing

Samples from viral DNA were purified with AMPure XP (Beckman Coulter Inc., Brea, CA, USA) beads kit to remove residual cellular DNA and sent for sequencing to the GenomEast platform (IGBMC Microarray and Sequencing platform, Illkirch-Graffenstaden, France). Data from Illumina HiSeq4000 (Illumina Inc., San Diego, CA, USA) in 2x100bp paired-end runs were quality trimmed using custom scripts written in Perl and R. Pairs with at least one read having more than 5 bases with a Phred quality score < 13 were discarded at this step. The filtered reads were then mapped using the Burrows-Wheeler Alignment tool [51] against the genome of the host cells used for virus production, and the pairs properly mapped with a high mapping score were considered as contaminant and discarded. This step was particularly important for samples with high proportion of contaminating DNA from host cell genomes. Contigs were de novo assembled with SPAdes v3.11.1 [52] following authors instructions and

scaffolding was performed with custom script to generate the longest consensus sequence for each viral genome. Open reading frames (ORFs) longer than 150 nt were automatically annotated, and a custom script written in python3 and based on the Dijkstra algorithm was used to identify homologous regions between PoxSTG and each of the parental strains. Global pairwise alignments were performed using MAFFT v7.017 to measure the genomic homology between PoxSTG and each parental genome, and to highlight the longest regions with strict identity between PoxSTG and the corresponding parental genome [53]. In addition, multiple alignments of the whole core-region of PoxSTG and the parental genomes was performed using Mauve to identify potential structural variants [54].

Generation of recombinant viruses

Single (TK)-deleted virus, named PoxSTG19508, was generated by insertion of the *GFP::FCU1* fusion gene into the PoxSTG *J2R* locus. Briefly, CEF were infected with PoxSTG at a MOI of 10^{-2} and incubated at 37°C for 2h, then transfected with a shuttle plasmid containing the *GFP::FCU1* fusion gene [50] under the control of the synthetic p11k7.5 promoter and surrounded by the flanking sequence of the VACV *J2R* gene. The cells were then incubated for 48h at 37°C. Double recombination occurred between *J2R* homologous regions in the shuttle plasmid and the parental virus, resulting in the insertion of the *GFP::FCU1* fusion gene into the *J2R* locus of PoxSTG. Recombinant virus, named PoxSTG19508, was isolated and submitted to additional plaque purification cycles on CEF. Insertion of the GFP::FCU1 sequence into the *TK* locus was confirmed by multiple PCRs and DNA sequencing. The same methods were used to generate the double (TK/RR)-deleted virus, named PoxSTG19730, by homologous recombination between PoxSTG19508 and a shuttle plasmid containing the *mCherry* gene under the control of the pH5R promoter and surrounded by the flanking sequence of the VACV *I4L* gene. For generation of the double (TK/RR)-deleted virus expressing murine IL-12 (mIL-12) and renamed PoxSTG19847, mCherry was replaced by mIL-12 by homologous recombination between PoxSTG19730 and a shuttle plasmid containing the *mIL-12* gene under the control of the pH5R promoter. Single (TK)-deleted Copenhagen strain virus, named CopTG17111, was generated by insertion of the *GFP::FCU1* fusion gene into the *J2R* locus. Double (TK/RR)-deleted virus Copenhagen strain virus expressing mIL-12 and named CopTG19328 was generated by insertion of the *mIL-12* gene, under the control of the pH5R promoter, into the *I4L* locus. Single thymidine kinase (TK)-deleted orthopoxviruses—including VACV (VACV) strains WR (WRTG15467) and Wyeth (WYTG18254), as well as rabbitpox virus (RPXV; RPXTG19095)—were generated by insertion of the *GFP* gene into the *J2R* locus.

Recombinant viruses were amplified in CEF and purified, and virus stocks were titrated on Vero cells by plaque assay.

***In vitro* cytotoxicity assay**

The viral lytic capacity was measured using the trypan blue exclusion method. Human tumor cells were transduced in suspension by respective chimeric viruses at the indicated MOI. A total of 3 x 10^5 cells/well were plated in 6-well culture dishes in 2 ml of medium supplemented with 10% FCS. Cells were then cultured at 37°C for 4 or 5 days and the viable cells were counted by trypan blue exclusion using a Vi-Cell Cell Counter (Beckmann Coulter, CA, USA). All samples were analyzed in triplicate. Mock- infected cells served as negative control and established the 100% survival point for the given assay.

***In vitro* virus yield**

To evaluate viral replication in human tumor cells and human primary cells, Hep G2 cells and hepatocytes were infected in 6-well plates at MOI 10^{-5} and MOI 10^{-4}, respectively (in triplicate). Three days after infection, supernatants and cells were collected, freeze thawed, sonicated, and viral progeny was quantified on Vero cells by plaque assay. To evaluate viral replication in a reconstructed human skin model, culture of Phenion full-thickness skin model was infected with the indicated virus at 10^5 PFU (in triplicate). Cultures were incubated for 7 days at 37°C. Viral progeny in reconstructed skin were quantified on Vero cells by plaque assay after 2 cycles of sonication in PBS. To quantify the infectious EEV and IMV at early times after infection, confluent A549 cells (1 x 10^6 cells) were infected in 6-well plates at MOI 10^{-1} for 1 h (in triplicate). Cells were then washed with PBS and replaced with fresh medium and incubated for 16 or 24 hours. Supernatants and cell fractions were collected separately. The supernatants were used to quantify EEV. The cell fractions were harvested in 1 mL PBS and the cell-associated virions, namely IMV, were extracted from cell lysates by freeze-thawing and sonication. Both virions (EEV and IMV) were titrated on Vero cells by plaque assay.

Cytosine deaminase enzymatic assay

Cytosine deaminase (CDase) activity was quantified by measuring the amount of 5-FU released in the culture media. A549 cells were infected with the different vectors at a MOI of 10^{-4} (in triplicate) and plated in 6-well culture dish (3 x 10^5 cells/well). After 6 hours, 1 mM 5-FC was added to the culture medium. From day 1 to day 3 post-infection, 5-FC and 5-FU concentrations in the media were measured by HPLC. Fifty µL of media were quenched with 50 µL of acetonitrile. The samples were vortexed and centrifuged. The organic supernatant was evaporated to dryness and reconstituted in 50 µL of water and analyzed by HPLC using a mobile

phase of 50 mM phosphoric acid adjusted to pH 2.1. Results are expressed as the percentage of 5-FU relative to the total amount of 5FC + 5FU after various incubation times with 5-FC.

Syncytia formation assay

VACV Copenhagen strain and the chimeric poxvirus were tested for syncytia formation in the HCT116 human CRC cell line. HCT116 cells were infected with CopTG17111 and PoxSTG19508 at a MOI of 10^{-3} and plated in 6-well culture dish (3 x 10^5 cells/well). Cells were observed by optical and fluorescence microscopy at 48 and 72 hours post-infection.

Comet assays

A549 cells were seeded in 60 mm tissue culture dishes and grown to near confluence overnight. The following day, cell monolayers were rinsed with PBS and inoculated with approximately 40 plaque-forming units (PFU) of virus in 500 µL of PBS supplemented with 2% fetal calf serum (FCS) and 1% cations. Cells were incubated for 1 h at 37°C to allow viral adsorption. After incubation, monolayers were rinsed and overlaid with 5 mL of growth medium. At 2 days post-infection, plaques were imaged using a Nikon SMZ18 fluorescence microscope (for GFP-expressing viruses). Subsequently, cell monolayers were stained with crystal violet (stock solution diluted 1:40 in ethanol) for plaque visualization.

***In vitro* cell pyroptosis determination**

For cell morphology analysis, HCT116 and A549 cells were infected with CopTG17111 or PoxSTG19508 at a MOI of 10^{-1} and seeded in 6-well culture plates at a density of 3×10^5 cells per well. Cell morphology was examined by optical microscopy at 48 hours post-infection. Bright-field images were acquired to document characteristic cytopathic effects, including cell swelling and bubble formation. For secretion assays, HCT116 cells were infected with VVCop or PoxSTG at an MOI of 10^{-2}. Cell culture supernatants were collected at 24 and 48 hours post-infection. Release of LDH (Cytotoxicity Assay, Promega, Madison, WI, USA), IL-18 (Human IL-18 Quantikine ELISA Kit, R&D Systems, Minneapolis, MN, USA), HMGB1 (Human HMGB1 ELISA Kit, IBL International GmbH, Hamburg, Germany) and ATP (ATP Bioluminescence Assay Kit, Sigma-Aldrich, St. Louis, MO, USA) was quantified according to the manufacturers' protocols. For western blotting analysis, HCT116 and A549 cells were infected with the indicated viruses at a MOI of 10^{-3}, except for the non-propagative MVA, which was used at an MOI of 10^{-1}. At 48 hours post-infection, cells were washed with PBS and lysed in 300 µL of lysis buffer. Protein lysates (20 µg per sample) were resolved on NuPAGE 4–12% Bis-Tris gels (Invitrogen, Carlsbad, CA, USA), transferred onto PVDF membranes (Millipore, Burlington, MA, USA), and immunoblotted with the antibodies specified in the Fig. legends, following the manufacturers' instructions. The following primary antibodies were

used: Gasdermin E (Abcam, Cambridge, UK; ab215191; 1:1000), Caspase-3 (Cell Signaling Technology, Danvers, MA, USA; #9662; 1:1000), GAPDH (Abcam, Cambridge, UK; ab245357; 1:2000).

Neutralization assays

To assess complement-mediated neutralization, the VACV Copenhagen strain and the chimeric poxvirus were incubated at a concentration of 2×10^5 PFU for 1 hour at 37 °C in normal human serum (Sigma-Aldrich, Darmstadt, Germany) diluted to a final concentration of 20%. Residual infectious virus was quantified by plaque assay on Vero cells. As a control for complement inactivation, viruses were incubated under identical conditions with heat-inactivated human serum (56°C for 1 hour), and infectious titers were determined as described above. To assess antibody-mediated neutralization, the oncolytic activity of the VACV Copenhagen strain and the chimeric poxvirus was tested in the presence of serum samples collected before and after intravenous administration of VACV TG6002 (patient) or PoxSTG19730 (dog). HCT116 colorectal carcinoma cells were seeded in 96-well plates at a density of 1 x 10^4 cells per well. Cells were infected in triplicate with the indicated viruses at various multiplicities of infection (MOIs). Prior to infection, viral inocula were incubated for 1 hour at 37 °C in phosphate-buffered saline (PBS) with either patient serum (diluted 1:100) or dog serum (diluted 1:10). At 3 or 4 days post-infection, cell viability was assessed using the CellTiter-Blue Cell Viability Assay (Promega, Madison, WI, USA), following the manufacturer's protocol. Fluorescence was measured using a Tecan Infinite M1000 Pro microplate reader (excitation: 560 nm; emission: 590 nm). Viability was expressed as a percentage relative to mock-infected controls. The half-maximal effective concentration (EC_{50}) was calculated by fitting a sigmoidal dose–response curve using GraphPad Prism software (GraphPad Software, San Diego, CA, USA).

Animal studies

For human xenograft tumor models, 5 x 10^6 human cancer cells (HCT116 and Hep G2) were injected subcutaneously into the flank of Swiss nude mice (Charles River Laboratories, Ecully, France). When the tumors reached a volume of 100-200 mm^3, the mice were randomized in a blinded manner and treated once intravenously with the indicated vectors. For bilateral tumor model, 5 x 10^6 human cancer HCT116 cells were injected on both sides of the flank of Swiss nude. When the tumors reached a diameter of 100-200 mm^3, the mice were randomized in a blinded manner and the virus was injected once intratumorally in the right-side tumor. For syngeneic murine tumor models, 2×10^5 CT26 cells or 3×10^5 B16F10 cells were injected subcutaneously into the flank of BALB/c mice or C57BL/6 mice, respectively (Charles River Laboratories, Ecully, France). When tumors became palpable, the mice were randomized in a

blinded manner and treated intratumorally or intravenously with the indicated vectors. Tumor size was measured twice weekly using calipers. Tumor volumes were calculated in cubic millimeters using the formula ($\pi/6$) x (length x width^2). The animals were euthanized when their tumor volumes reached 2 000 mm^3. For bilateral tumor model, mice were euthanized when total volume of both tumors exceeded 2000 mm^3. To assess the amount of virus in tumors, tumors were collected and weighed, homogenized in PBS, sonicated, and titers were determined on Vero cells by plaque assay.

Immunohistochemical analysis

Tumors were collected, formalin fixed, paraffin-embedded and sectioned. Sections (5 µM) were mounted on adhesive glass slides and used for histological analysis. Virus-infected cells were detected upon incubation of the slide with rabbit IgG anti-VACV (Meridian Bioscience, Cincinnati, OH, USA; B65101R) at a dilution of 1:1400 and the antibody-binding signal was detected by using the NovoLink Polymer Detection System (Leica Microsystems, Wetzlar, Germany). Signals were visualized with the TSA-fluorescein pack (Akoya Biosciences, Marlborough, MA, USA; SAT701001EA) and counterstained with DAPI (Sigma-Aldrich, St. Louis, MO, USA; B-2883). Stained slides were scanned by a high-resolution fluorescent slide scanner (NanoZoomer, Hamamatsu Photonics, Hamamatsu, Japan) and quantification of the signal was done using the Calopix software (TRIBVN Healthcare, Châtillon, France). Virus-infected cells were expressed as a proportion of total tumor area.

ELISpot Assay

Mice bearing subcutaneous murine colon carcinoma CT26 tumors were treated intratumorally with a single dose of CopTG17111 or PoxSTG19508 at 1 x 10^7 PFU. Six days post-injection, mice were euthanized and spleens collected. Splenocytes were isolated by density gradient centrifugation on Lympholyte-M (Cedarlane Laboratories, Burlington, ON, Canada) followed by red blood cell lysis using BD Pharm Lyse Lysing Buffer (1x) (BD Biosciences, Franklin Lakes, NJ, USA). Mononuclear cells were plated in 96-well MultiScreen-IP (MSIP) plates (Millipore, Burlington, MA, USA) pre-coated with anti-IFN-γ capture antibody (Mabtech AB, Nacka Strand, Sweden) and stimulated with 1 µg/mL of either an irrelevant peptide (TPHPARIGL), the vaccinia-specific S9L8 peptide (SPGAAGYDL), or the tumor-associated AH1 peptide (SPSYVYHQF). Plates were incubated for 18 h, washed, and immunospots revealed using biotinylated anti-IFN-γ detection antibody (Mabtech AB, Nacka Strand, Sweden), ExtrAvidin–alkaline phosphatase (Sigma-Aldrich, St. Louis, MO, USA), and BCIP/NBT substrate (Sigma-Aldrich, St. Louis, MO, USA). Spots were counted using an ImmunoSpot S5 UV Analyzer (Cellular Technology Limited, Shaker Heights, OH, USA).

Statistical analysis

In vitro, data were analyzed by one-way analysis of variance (ANOVA) followed by post-hoc tests using Tukey adjustment. Statistical analyses of tumor volume growth were performed, using a mixed model to take the longitudinal aspect into account [15]. The inter-individual heterogeneity was considered as a random effect in the model. Tumor sizes were converted in equivalent diameters to comply with the mixed model assumption and to get a better fit to the statistical model [55]. Comparisons between treatments were also performed using least-squares means. To study non-inferiority relations, overall estimation of tumor size growth with the associated interval of measurement uncertainty was compared. Survival analyses were performed using log-rank test. For ELISpot analysis, general linear models were used to evaluate differences in the mean spot forming units between treatment groups and pairwise comparisons between groups were performed using Tukey's correction. Statistical analyses were performed using R software. Differences were considered statistically significant at $p < 0.05$, with significance levels denoted as follows: $p < 0.05$ (*), $p < 0.01$ (**), $p < 0.001$ (***), and $p < 0.0001$ (****).

Ethics statement

The mouse studies were approved by the Comité d'éthique en matière d'expérimentation animale de Strasbourg (CREMEAS) and were conducted in accordance with local legislation and institutional requirements. The dog study was approved by VetAgro Sup Ethics Committee and was conducted at Biovivo – VetAgro Sup in accordance with Biovivo's standard operating procedures and in full compliance with European regulations on animal experimentation.

Author contributions

Conceptualization: PE. Investigation: JF, AF, JD, IF, CP, JK, MK, JH, BM, SC, BG, PE. Data analysis: JF, JD, BG, PE. Writing-original draft: PE. Writing-revised draft: JF, JD, BG. Supervision: JF, PE.

Acknowledgments

We thank Virginie Nourtier and Murielle Gantzer (Transgene) for preparing tumor cells for injection into mice and Laurence Laruelle and Berangere Bastien (Transgene) for the statistical analyses.

Disclosure and competing interest statement

All authors were employees and shareholders of Transgene SA. The authors declare that no financial support was received for the research and/or publication of this article. A.F. and P.E. are listed as inventors on a patent application (WO 2024/038175 A1) submitted by Transgene and related to this work.

References

1. Kaufman, H.L., Kohlhapp, F.J. & Zloza, A. Oncolytic viruses: a new class of immunotherapy drugs. *Nat Rev Drug Discov* **14**, 642-662 (2015).
2. Khuri, F.R. et al. a controlled trial of intratumoral ONYX-015, a selectively-replicating adenovirus, in combination with cisplatin and 5-fluorouracil in patients with recurrent head and neck cancer. *Nat Med* **6**, 879-885 (2000).
3. Foloppe, J. et al. TG6002 oncolytic vaccinia virus and chemotherapy synergy: a promising strategy for pancreatic ductal adenocarcinoma. *Front Microbiol* **16**, 1656984 (2025).
4. Puzanov, I. et al. Talimogene Laherparepvec in Combination With Ipilimumab in Previously Untreated, Unresectable Stage IIIB-IV Melanoma. *J Clin Oncol* **34**, 2619-2626 (2016).
5. Rosewell Shaw, A. et al. Adenovirotherapy Delivering Cytokine and Checkpoint Inhibitor Augments CAR T Cells against Metastatic Head and Neck Cancer. *Mol Ther* **25**, 2440-2451 (2017).
6. Tanoue, K. et al. Armed Oncolytic Adenovirus-Expressing PD-L1 Mini-Body Enhances Antitumor Effects of Chimeric Antigen Receptor T Cells in Solid Tumors. *Cancer Res* **77**, 2040-2051 (2017).
7. Pol, J., Kroemer, G. & Galluzzi, L. First oncolytic virus approved for melanoma immunotherapy. *Oncoimmunology* **5**, e1115641 (2016).
8. Stavrakaki, E., Everts, A., van den Hoogen, B.G. & Lamfers, M.L.M. The 16th International Oncolytic Virus Conference: Advancing oncolytic virotherapy by balancing anti-tumor and anti-viral immunity. *Mol Ther Oncol* **33**, 200950 (2025).
9. Grier, A.L. et al. Recent Advances in Immunotherapy for Non-Muscle-Invasive Bladder Cancer. *Cancers (Basel)* **18** (2026).
10. Xia, Y., Li, D., Yang, K. & Ou, X. Systemic Delivery Strategies for Oncolytic Viruses: Advancing Targeted and Efficient Tumor Therapy. *Int J Mol Sci* **26** (2025).
11. Omolekan, T.O. et al. Viral warfare: unleashing engineered oncolytic viruses to outsmart cancer's defenses. *Front Immunol* **16**, 1618751 (2025).
12. Fenner, F. Risks and benefits of vaccinia vaccine use in the worldwide smallpox eradication campaign. *Res Virol* **140**, 465-466; discussion 487-491 (1989).
13. Stawowczyk, M., Ye, Y. & Chen, N.G. Vaccinia Virus-A Swiss Army Knife Against Cancer. *Cancers (Basel)* **17** (2025).
14. Xu, L., Sun, H., Lemoine, N.R., Xuan, Y. & Wang, P. Oncolytic vaccinia virus and cancer immunotherapy. *Front Immunol* **14**, 1324744 (2023).
15. Foloppe, J. et al. The Enhanced Tumor Specificity of TG6002, an Armed Oncolytic Vaccinia Virus Deleted in Two Genes Involved in Nucleotide Metabolism. *Mol Ther Oncolytics* **14**, 1-14 (2019).

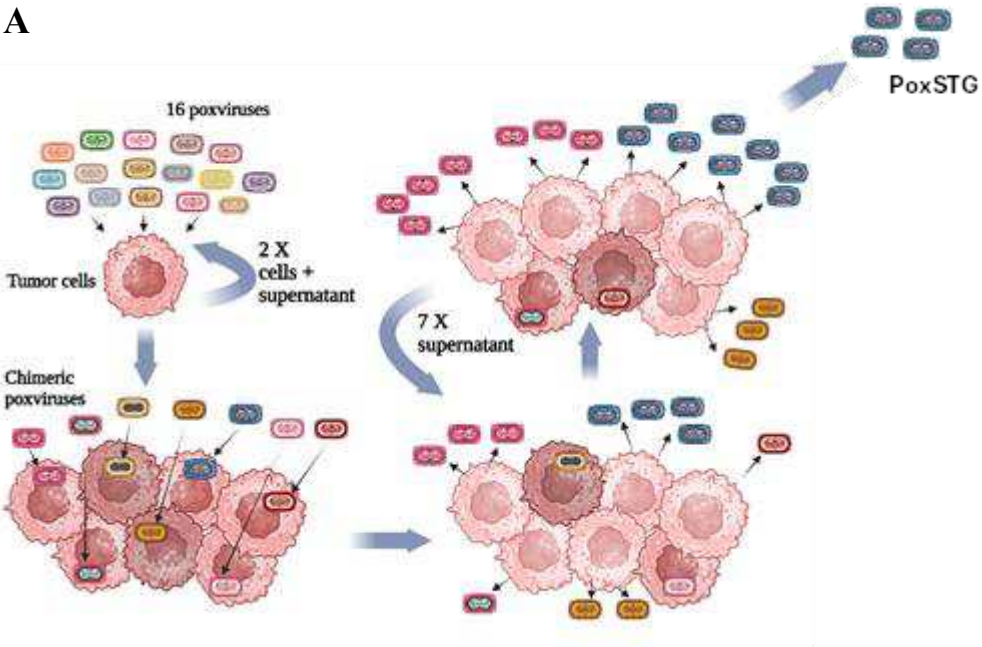
16. Erbs, P. et al. In vivo cancer gene therapy by adenovirus-mediated transfer of a bifunctional yeast cytosine deaminase/uracil phosphoribosyltransferase fusion gene. *Cancer research* **60**, 3813-3822 (2000).
17. Cassier, P. et al. in ESMO Congress 2021, Vol. 32 S530–S582 (Annals of Oncology, 2021).
18. West, E.J. et al. A phase I clinical trial of intrahepatic artery delivery of TG6002 in combination with oral 5-fluorocytosine in patients with liver-dominant metastatic colorectal cancer. *Clin Cancer Res* (2025).
19. Beguin, J. et al. Oncolytic virotherapy with intratumoral injection of vaccinia virus TG6002 and 5-fluorocytosine administration in dogs with malignant tumors. *Mol Ther Oncolytics* **30**, 103-116 (2023).
20. Bauzon, M. & Hermiston, T.W. Oncolytic viruses: the power of directed evolution. *Adv Virol* **2012**, 586389 (2012).
21. Ricordel, M. et al. Vaccinia Virus Shuffling: deVV5, a Novel Chimeric Poxvirus with Improved Oncolytic Potency. *Cancers (Basel)* **10** (2018).
22. Ricordel, M. et al. Oncolytic properties of non-vaccinia poxviruses. *Oncotarget* **9**, 35891-35906 (2018).
23. O'Leary, M.P. et al. Novel oncolytic chimeric orthopoxvirus causes regression of pancreatic cancer xenografts and exhibits abscopal effect at a single low dose. *J Transl Med* **16**, 110 (2018).
24. Puhlmann, M. et al. Vaccinia as a vector for tumor-directed gene therapy: biodistribution of a thymidine kinase-deleted mutant. *Cancer gene therapy* **7**, 66-73 (2000).
25. Burton, C. & Bartee, E. Syncytia Formation in Oncolytic Virotherapy. *Mol Ther Oncolytics* **15**, 131-139 (2019).
26. Smith, G.L. & Vanderplasschen, A. Extracellular enveloped vaccinia virus. Entry, egress, and evasion. *Adv Exp Med Biol* **440**, 395-414 (1998).
27. DeHaven, B.C., Gupta, K. & Isaacs, S.N. The vaccinia virus A56 protein: a multifunctional transmembrane glycoprotein that anchors two secreted viral proteins. *J Gen Virol* **92**, 1971-1980 (2011).
28. Wagenaar, T.R. & Moss, B. Association of vaccinia virus fusion regulatory proteins with the multicomponent entry/fusion complex. *J Virol* **81**, 6286-6293 (2007).
29. Wagenaar, T.R., Ojeda, S. & Moss, B. Vaccinia virus A56/K2 fusion regulatory protein interacts with the A16 and G9 subunits of the entry fusion complex. *J Virol* **82**, 5153-5160 (2008).
30. Leroy, H. et al. Virus-Mediated Cell-Cell Fusion. *Int J Mol Sci* **21** (2020).
31. Guedan, S. et al. GALV expression enhances the therapeutic efficacy of an oncolytic adenovirus by inducing cell fusion and enhancing virus distribution. *Gene Ther* **19**, 1048-1057 (2012).
32. Ayala-Breton, C., Russell, L.O., Russell, S.J. & Peng, K.W. Faster replication and higher expression levels of viral glycoproteins give the vesicular stomatitis virus/measles virus hybrid VSV-FH a growth advantage over measles virus. *J Virol* **88**, 8332-8339 (2014).
33. Abdullahi, S. et al. A Novel Chimeric Oncolytic Virus Vector for Improved Safety and Efficacy as a Platform for the Treatment of Hepatocellular Carcinoma. *J Virol* **92** (2018).

34. McIntosh, A.A. & Smith, G.L. Vaccinia virus glycoprotein A34R is required for infectivity of extracellular enveloped virus. *J Virol* **70**, 272-281 (1996).
35. Smith, G.L., Vanderplasschen, A. & Law, M. The formation and function of extracellular enveloped vaccinia virus. *J Gen Virol* **83**, 2915-2931 (2002).
36. Riccardo, V. & Pablo, G.C. Neutralization Determinants on Poxviruses. *Viruses* **15** (2023).
37. Loveless, R., Bloomquist, R. & Teng, Y. Pyroptosis at the forefront of anticancer immunity. *J Exp Clin Cancer Res* **40**, 264 (2021).
38. Inkol, J.M. et al. Pyroptosis activates conventional type I dendritic cells to mediate the priming of highly functional anticancer T cells. *J Immunother Cancer* **12** (2024).
39. Shen, Z. et al. Improving the therapeutic efficacy of oncolytic viruses for cancer: targeting macrophages. *J Transl Med* **21**, 842 (2023).
40. Zhang, Y. et al. Coxsackievirus Group B3 Has Oncolytic Activity against Colon Cancer through Gasdermin E-Mediated Pyroptosis. *Cancers (Basel)* **14** (2022).
41. Lin, J. et al. Oncolytic Parapoxvirus induces Gasdermin E-mediated pyroptosis and activates antitumor immunity. *Nat Commun* **14**, 224 (2023).
42. Zhao, Z. et al. Zika virus causes placental pyroptosis and associated adverse fetal outcomes by activating GSDME. *Elife* **11** (2022).
43. Wang, Y. et al. Chemotherapy drugs induce pyroptosis through caspase-3 cleavage of a gasdermin. *Nature* **547**, 99-103 (2017).
44. Chen, X.Y. et al. Arming oncolytic M1 virus with gasdermin E enhances antitumor efficacy in breast cancer. *iScience* **27**, 111148 (2024).
45. Chen, X. et al. Genetic engineering of systemically injectable oncolytic viruses for pyroptosis-accelerated cancer virotherapy. *Nat Cancer* (2026).
46. Minnar, C.M., Lui, G., Gulley, J.L., Schlom, J. & Gameiro, S.R. Preclinical and clinical studies of a tumor targeting IL-12 immunocytokine. *Front Oncol* **13**, 1321318 (2023).
47. Foloppe, J. et al. Targeted delivery of a suicide gene to human colorectal tumors by a conditionally replicating vaccinia virus. *Gene therapy* **15**, 1361-1371 (2008).
48. Erbs, P. et al. Modified vaccinia virus Ankara as a vector for suicide gene therapy. *Cancer gene therapy* **15**, 18-28 (2008).
49. Beguin, J. et al. Preclinical Evaluation of the Oncolytic Vaccinia Virus TG6002 by Translational Research on Canine Breast Cancer. *Mol Ther Oncolytics* **19**, 57-66 (2020).
50. Ricordel, M. et al. Cowpox Virus: A New and Armed Oncolytic Poxvirus. *Mol Ther Oncolytics* **7**, 1-11 (2017).
51. Li, H. & Durbin, R. Fast and accurate short read alignment with Burrows-Wheeler transform. *Bioinformatics* **25**, 1754-1760 (2009).
52. Nurk, S. et al. Assembling single-cell genomes and mini-metagenomes from chimeric MDA products. *J Comput Biol* **20**, 714-737 (2013).
53. Katoh, K., Misawa, K., Kuma, K. & Miyata, T. MAFFT: a novel method for rapid multiple sequence alignment based on fast Fourier transform. *Nucleic Acids Res* **30**, 3059-3066 (2002).
54. Darling, A.C., Mau, B., Blattner, F.R. & Perna, N.T. Mauve: multiple alignment of conserved genomic sequence with rearrangements. *Genome Res* **14**, 1394-1403 (2004).

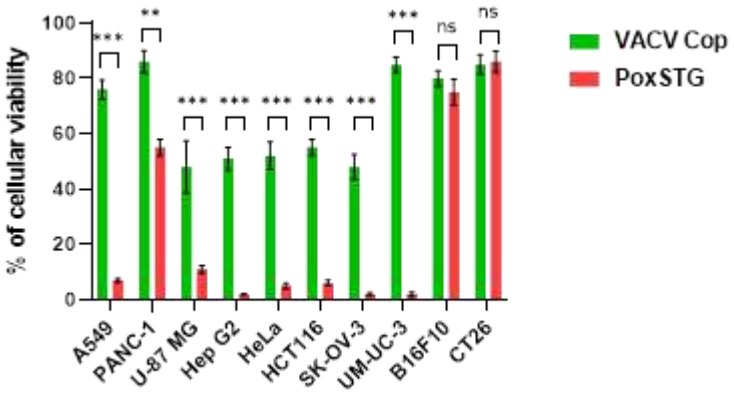
55. Bastogne, T. et al. Phenomenological modeling of tumor diameter growth based on a mixed effects model. *J Theor Biol* **262**, 544-552 (2010).

Figure 1

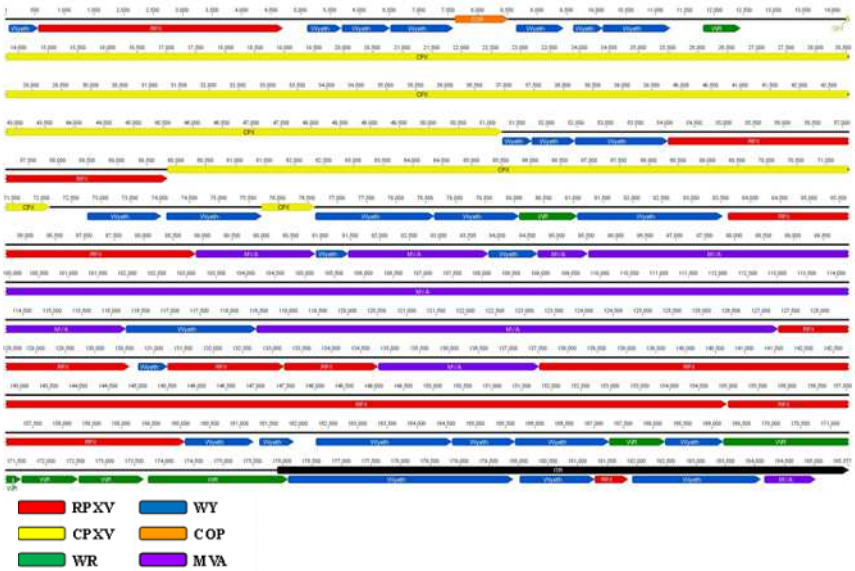
A



B



C



D

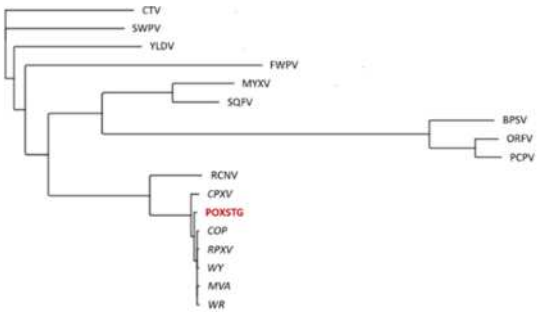


Figure 1. Directed evolution generated a chimeric poxvirus with improved oncolytic potency. (**A**) Schematic illustration of the directed evolution workflow used to select chimeric poxviruses. Sixteen distinct poxviruses (COP, WY, WR, MVA-GFP, CPXV, RCNV, RPXV, BPSV, ORFV, PCPV, MYXV, YLDV, SWPV, CTV, SQFV, FWPV) were combined and used to infect A549 cells at a multiplicity of infection (MOI) of 10^{-2} per virus. The mixed viral population was sequentially passaged on confluent A549 cells in T75 flasks for nine passages. Beginning at passage 3, supernatants were subjected to 10-fold serial dilutions and used to infect fresh flasks; the least concentrated dilution that did not induce a strong cytopathic effect was harvested at 24 h post-infection. After passage 9, 48 plaque-purified viral clones were isolated, amplified, titrated, and subsequently evaluated for oncolytic activity on A549 tumor cells. (**B**) Oncolytic effect of PoxSTG across a panel of tumor cell lines. Human tumor cell lines (infected at MOI 10^{-5}) and murine tumor cell lines (MOI 10^{-3}) were infected with PoxSTG. Cell viability was measured 5 days post-infection using trypan blue exclusion. The parental VACV Copenhagen strain (COP) was used as reference. Data represent mean ± SD from three independent experiments. Statistical analysis was performed using one-way ANOVA; significance is indicated as ns (not significant), $p < 0.01$ (**), and $p < 0.001$ (***). (**C**) Genomic map of PoxSTG displaying the origin of each genomic region. Segments are color-coded according to their respective parental virus, with annotations highlighting the longest contiguous region sharing 100% sequence identity with each parental genome. The conserved PoxSTG core is indicated, along with its unique single inverted terminal repeat (ITR) in black. (**D**) Phylogenetic tree including PoxSTG and all viruses analyzed in this study. Viruses contributing genomic material to PoxSTG are indicated in italics. The tree was generated using a multiple sequence alignment method. Virus abbreviations: BPSV (Bovine Papular Stomatitis virus), COP (Vaccinia virus Copenhagen strain), CPXV (Cowpox virus), CTV (Cotia virus), FWPV (Fowlpox virus), MVA (Modified Vaccinia Ankara), MYXV (Myxoma virus), ORFV (ORF virus), PCPV (Pseudo-cowpox virus), RCNV (Raccoonpox virus), RPXV (Rabbitpox virus), SQFV (Squirrel Fibroma virus), SWPV (Swinepox virus), WR (Vaccinia virus Western Reserve strain), WY (Vaccinia virus Wyeth strain), YLDV (Yaba-like disease virus).

Figure 2

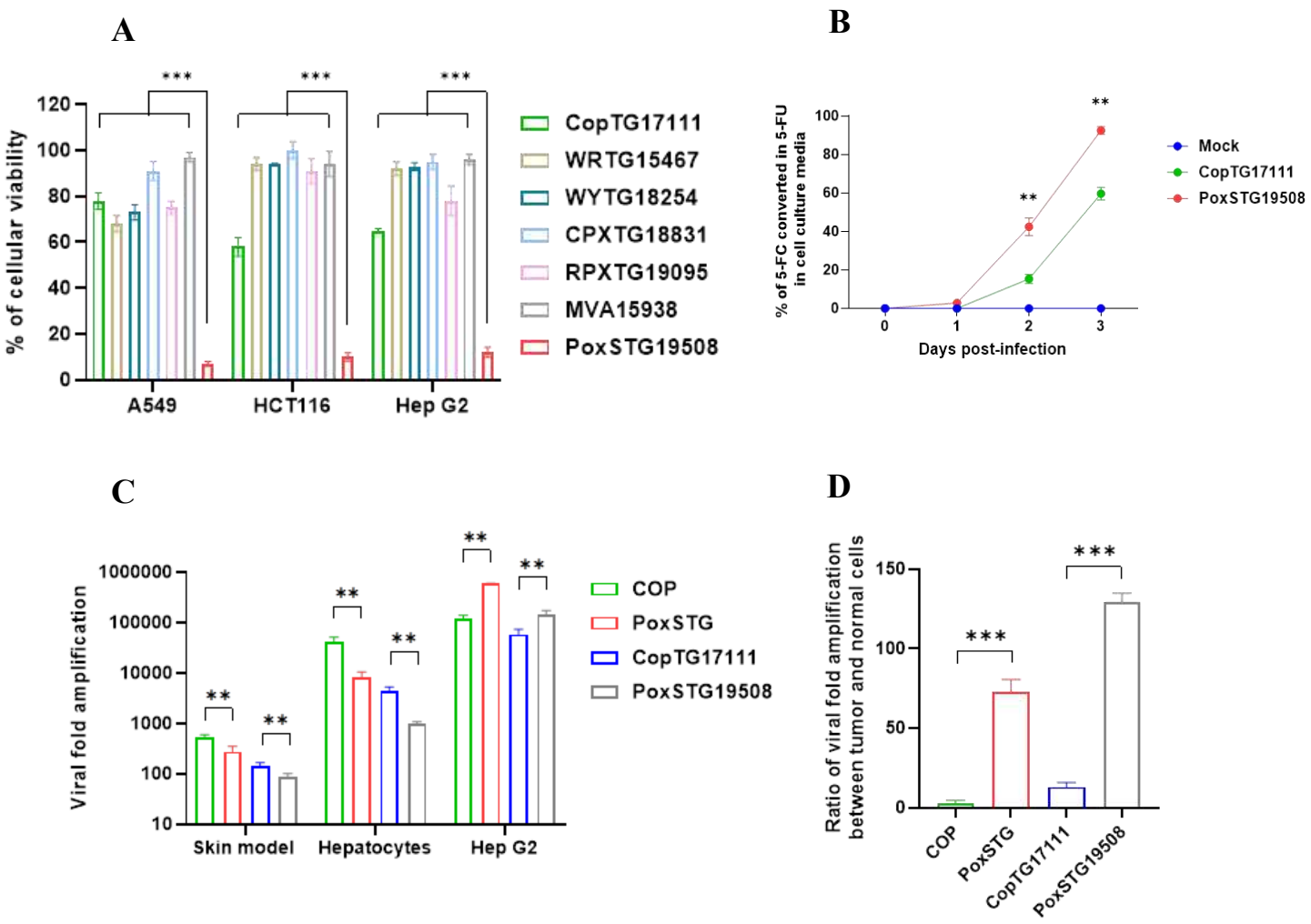
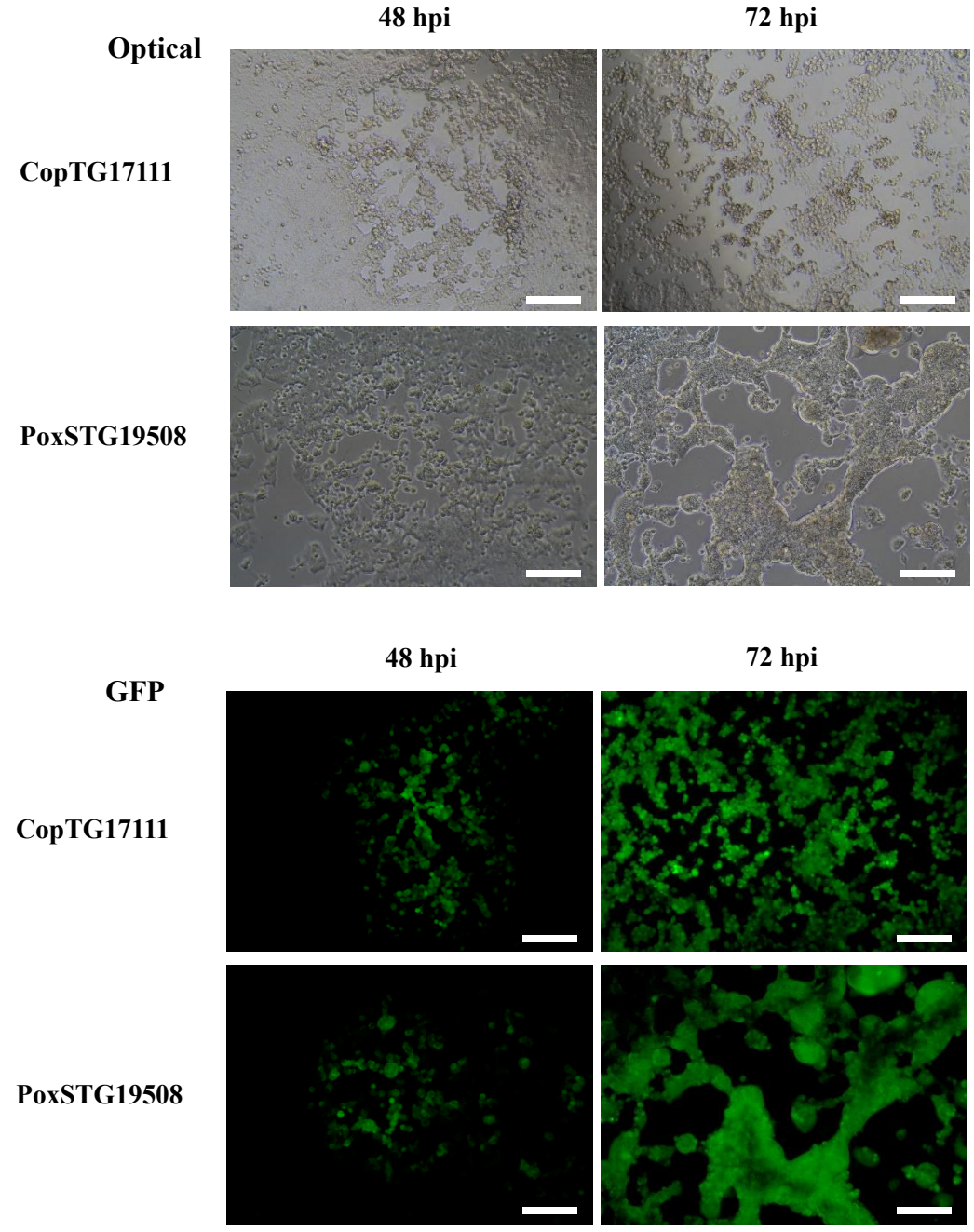


Figure 2. PoxSTG increases tumor cell destruction and transgene expression, with reduced replication in primary non-tumor cells. (**A**) Oncolytic activity of PoxSTG versus parental strains. Oncolytic potency of the TK-deleted chimeric virus PoxSTG19508, MVA, and TK-deleted parental strains was evaluated in A549, HCT116, and Hep G2 tumor cell lines infected at MOI 10^{-5}. Cell viability was measured 4 days post-infection by trypan blue exclusion. Data represent mean ± SD of triplicate experiments. One-way ANOVA: $p < 0.001$ (***). (**B**) FCU1 functionality and prodrug conversion by PoxSTG. A549 cells were infected at MOI 10^{-4} and exposed to 1 mM 5-FC at 6 h post-infection. Conversion of 5-FC into 5-FU and release of 5-FU into the supernatant were quantified by HPLC from days 1–3. Results are expressed as % of 5-FU relative to total 5-FC + 5-FU. Data represent mean ± SD ($n = 3$). One-way ANOVA: PoxSTG19508 vs CopTG17111 $p < 0.01$ (**). (**C**) Replication in tumor

cells and primary human models. Viral amplification was measured in Hep G2 cells (MOI 10^{-5}, harvest at day 3), primary human hepatocytes (MOI 10^{-4}, day 3), and 3D Phenion FT skin models (1×10^5 PFU, day 7). Viral progeny was quantified by plaque titration and expressed as fold amplification (output/input). Data represent mean ± SD (n = 3). (**D**) The ratio of fold amplification in Hep G2 versus hepatocytes (derived from panel C) is shown. One-way ANOVA: $p < 0.01$ (**), $p < 0.001$ (***).

Figure 3

A


48 hpi
72 hpi
Optical
CopTG17111
PoxSTG19508
48 hpi
72 hpi
GFP
CopTG17111
PoxSTG19508

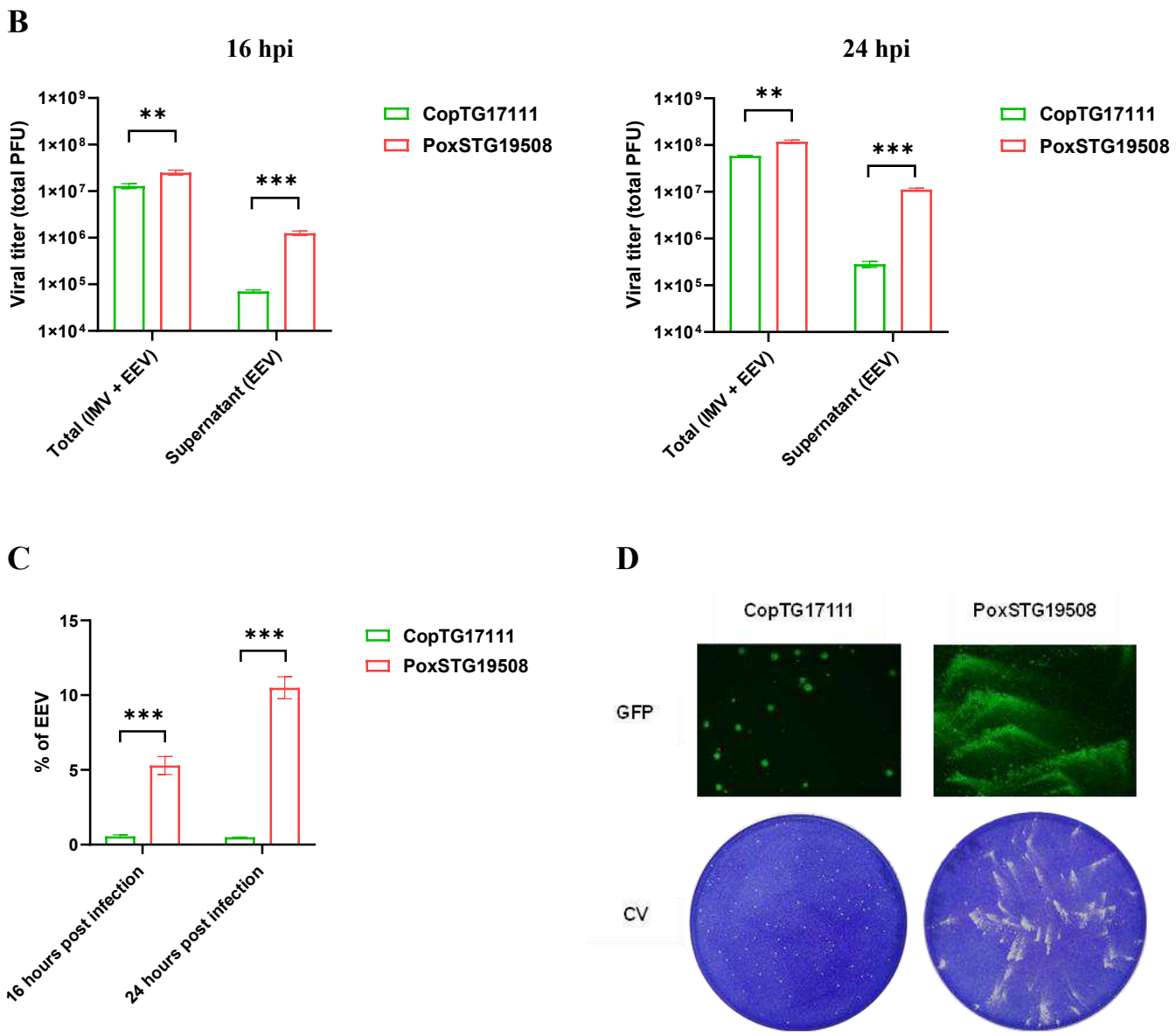
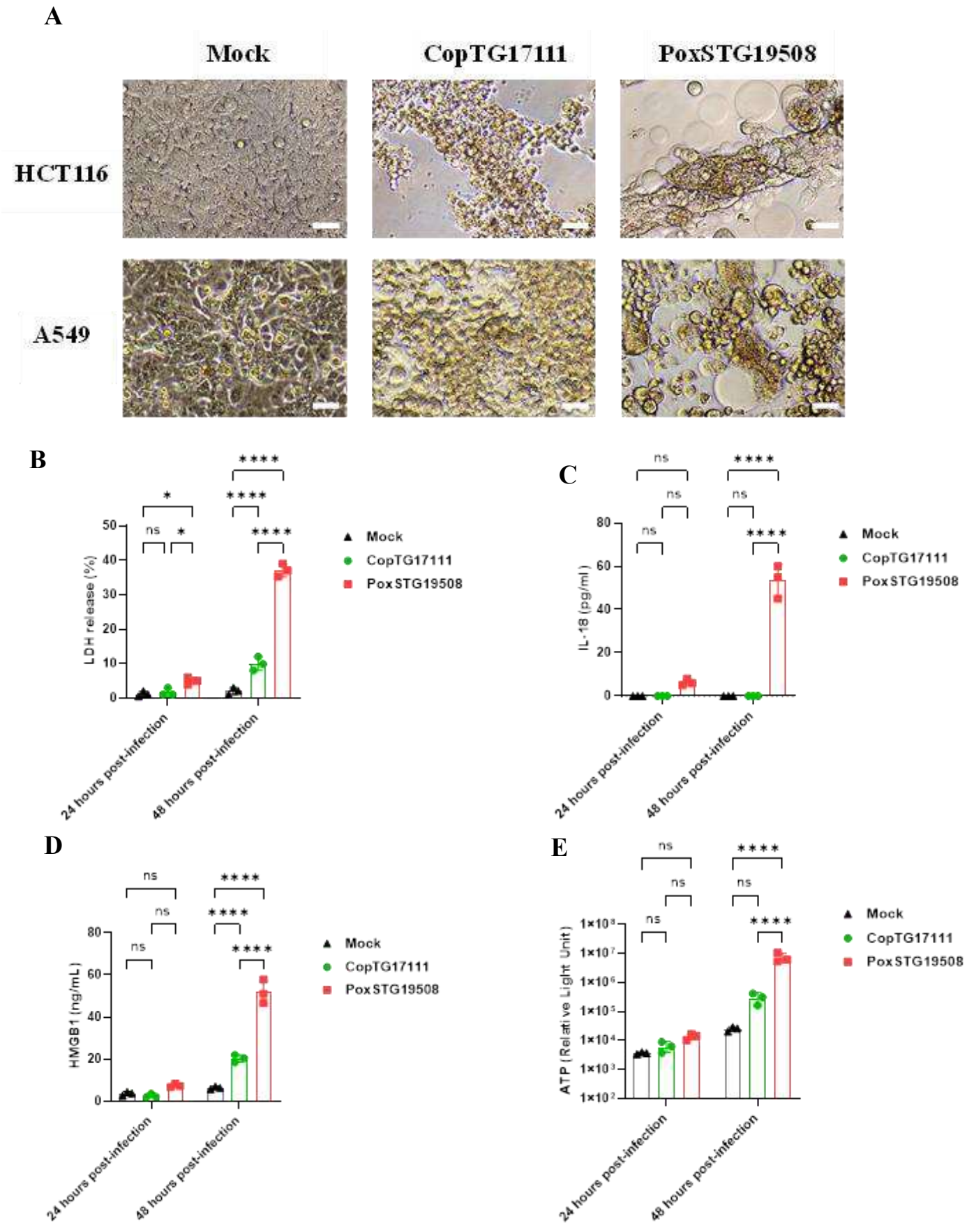


Figure 3 | PoxSTG induces syncytia formation and enhances EEV production.

(**A**) HCT116 cells were infected with GFP-expressing CopTG17111 or PoxSTG19508 at a MOI of 10^{-3}. Cell morphology was examined by bright-field and fluorescence microscopy at 48 and 72 hours post-infection (hpi). PoxSTG19508 infection induced extensive syncytia formation, characterized by large multinucleated cells resulting from fusion of adjacent cells, whereas CopTG17111-infected cultures retained predominantly individual rounded cells without evidence of fusion. Scale bar, 200 µm. (**B,C**) A549 cells were infected with CopTG17111 or PoxSTG19508 at an MOI of 0.1. Supernatant and cell-associated fractions were collected at 16 and 24 hpi. Viral titers were determined for EEV (supernatant fraction) and total progeny virus (IMV + EEV; combined supernatant and cell fractions). (**B**) EEV and total progeny virus titers

at 16 and 24 hpi. (**C**) Ratio of EEV to total progeny virus at each time point. Data are presented as mean ± SD from three independent experiments. Statistical significance was determined by one-way ANOVA; $p < 0.01$ (**), $p < 0.001$ (***). (**D**) Representative comet-shaped plaques produced by the indicated viruses in A549 monolayers 48 hpi. Plaques were visualized by GFP fluorescence and subsequently stained with crystal violet (CV) to assess monolayer disruption and virus spread. PoxSTG19508 generated prominent comet-shaped plaques consistent with enhanced extracellular virus-mediated dissemination.

Figure 4


A
Mock
CopTG17111
PoxSTG19508
HCT116
A549
B
LDH release (%)
24 hours post-infection
48 hours post-infection
Mock
CopTG17111
PoxSTG19508
C
IL-18 (pg/ml)
D
HMGB1 (ng/mL)
E
ATP (Relative Light Unit)
ns
*
****

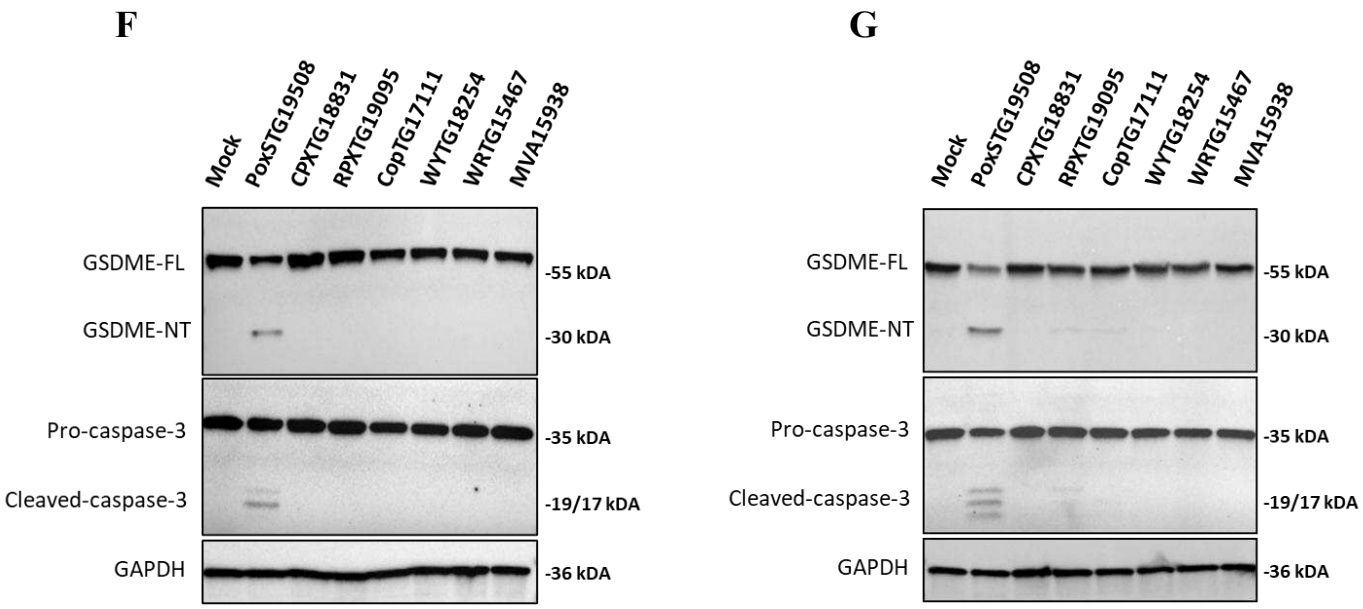
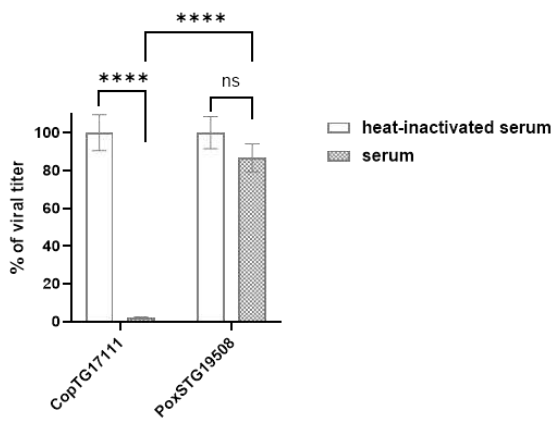


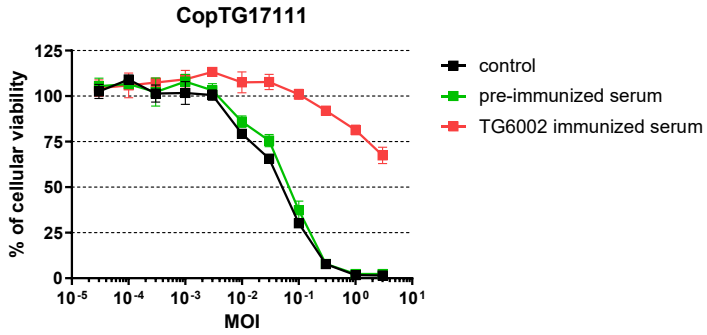
Figure 4. PoxSTG-induced pyroptotic cell death in tumor cells. (**A**) Morphological alterations of HCT116 and A549 cells two days post-infection at an MOI of 10^{-1} with the indicated viruses. Tumor cells treated with PoxSTG exhibited marked cell swelling and extensive membrane blebbing, with prominent bubble-like protrusions emerging from the cell surface (scale bar = 100 μm). (**B**–**E**) Release of LDH, IL-18, HMGB1 and ATP in HCT116 cells measured 24 and 48 h post-infection following treatment with CopTG17111 and PoxSTG19508 at an MOI of 10^{-2}. Data represent mean ± SD of three independent experiments. Statistical significance was assessed by one-way ANOVA; not significant (ns), $p < 0.05$ (*), $p < 0.0001$ (****). (**F**-**G**) Protein expression levels of GSDME-FL, GSDME-NT, pro-caspase-3, and cleaved caspase-3 in HCT116 (**F**) and A549 (**G**) cells 48 h post-infection with the indicated viruses at an MOI of 10^{-3}. GAPDH was used as a loading control.

Figure 5

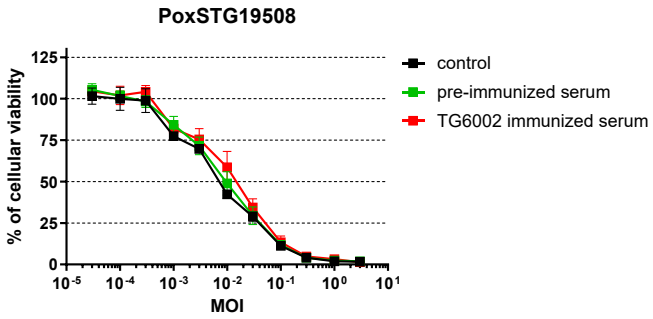
A



B



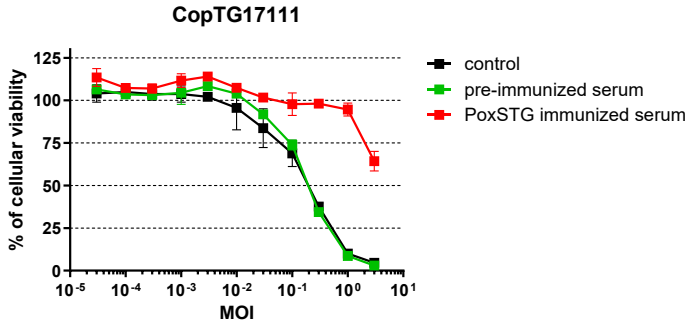
C



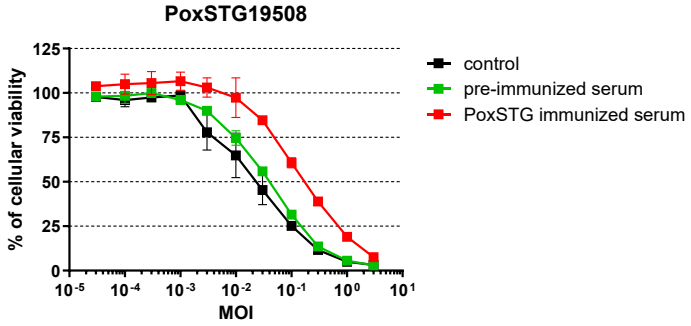
D

EC$_{50}$ (MOI)	Control (no serum)	Pre-immunized serum	TG6002 immunized serum
CopTG17111	4.9 x 10^{-2}	6.1 x 10^{-2}	7.6
PoxSTG19508	7.6 x 10^{-3}	9.7 x 10^{-3}	1.6 x 10^{-2}

E



F

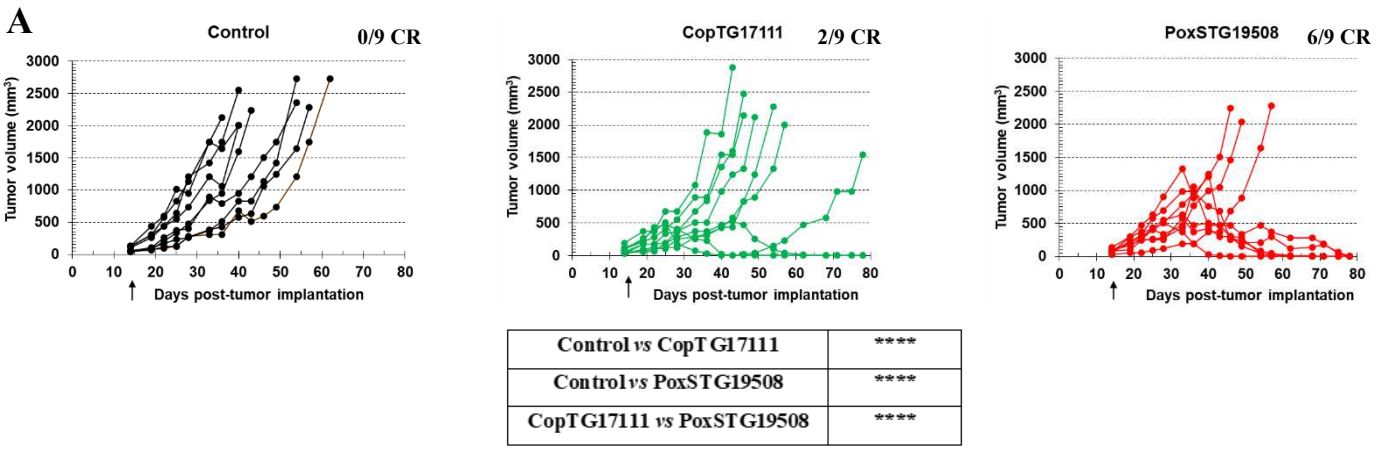


G

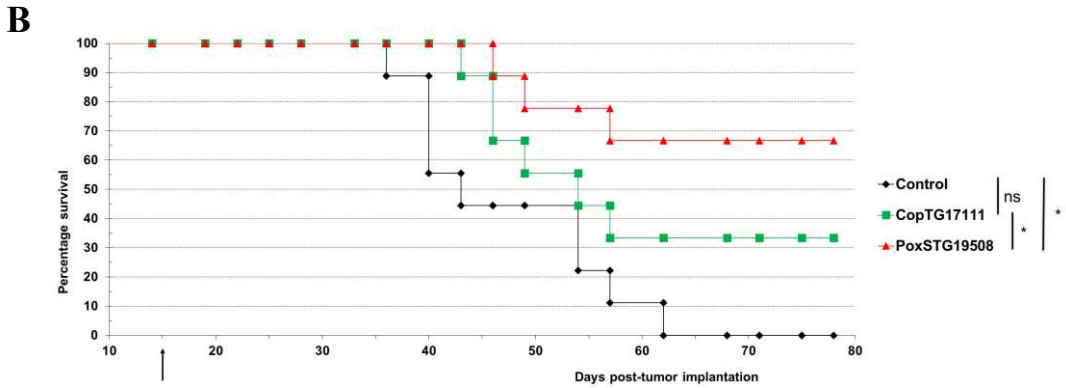
EC$_{50}$ (MOI)	Control (no serum)	Pre-immunized serum	PoxSTG immunized serum
CopTG17111	1.9 x 10^{-1}	1.9 x 10^{-1}	6.1
PoxSTG19508	2.2 x 10^{-2}	3.9 x 10^{-2}	1.6 x 10^{-1}

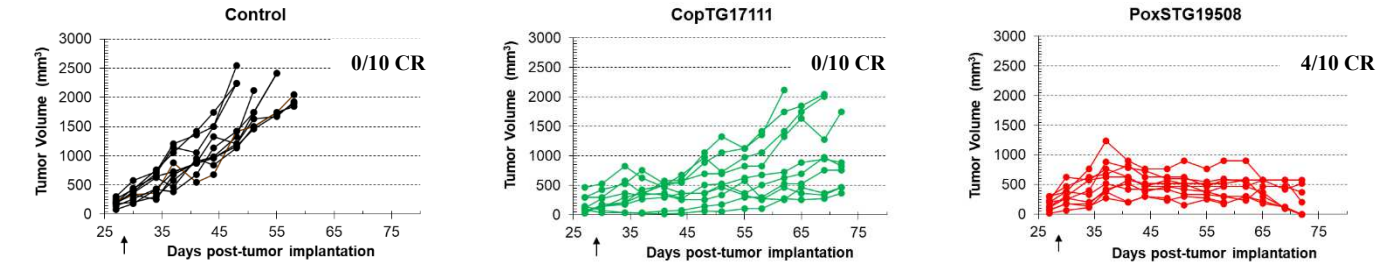
Figure 5. Neutralization escape of PoxSTG. (**A**) Sensitivity of COP and PoxSTG to complement-mediated neutralization in human serum. Viruses were incubated with 20 % of human serum for 1 hour, then used to inoculate Vero cells and incubated for 3 days to allow plaque formation. Plaque numbers are expressed as percentages relative to those obtained with heat-inactivated human serum. Data represent mean ± SD from three independent experiments. Statistical significance was determined by one-way ANOVA; not significant (ns), $p < 0.0001$ (****). (**B-G**) Antibody-mediated neutralization of COP and PoxSTG**.** Neutralization assays were performed using serum samples from (**B,C**) a patient treated with TG6002 or (**E,F**) a dog treated with PoxSTG. HCT116 cells were infected with CopTG17111 (**B, E**) or PoxSTG19508 (**C**, **F**) after preincubation with immunized serum collected post-intravenous administration of TG6002 (**B,C**) or PoxSTG19730 (**E,F**). Conditions without serum and with pre-immunized serum (collected before TG6002 or PoxSTG19730 administration) served as negative controls. The half-maximal effective concentration (EC_{50}) was determined by infecting HCT116 cells (10^4 cells/well, 96-well plate) with serial virus dilutions and assessing cell viability 4 days (**B,C**) or 3 days (**E,F**) post-infection using the CellTiter-Blue assay. Viability was normalized to uninfected controls. Data represent mean ± SD of triplicate experiments. (**D**) EC_{50} values were calculated from panels B and C; (**G**) EC_{50} values were calculated from panels E and F by fitting a sigmoidal dose–response curve.

Figure 6



Control *vs* CopTG17111	****
Control *vs* PoxSTG19508	****
CopTG17111 *vs* PoxSTG19508	****





Control *vs* CopTG17111	****
Control *vs* PoxSTG19508	****
CopTG17111 *vs* PoxSTG19508	****

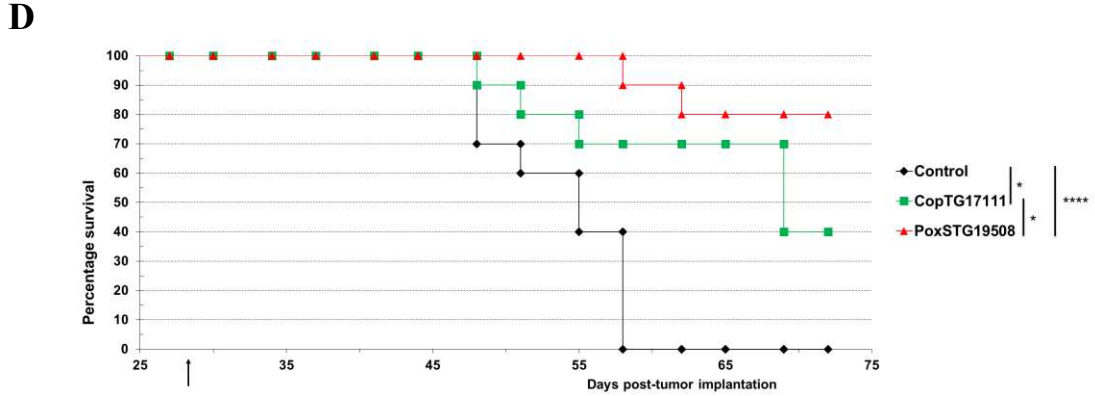
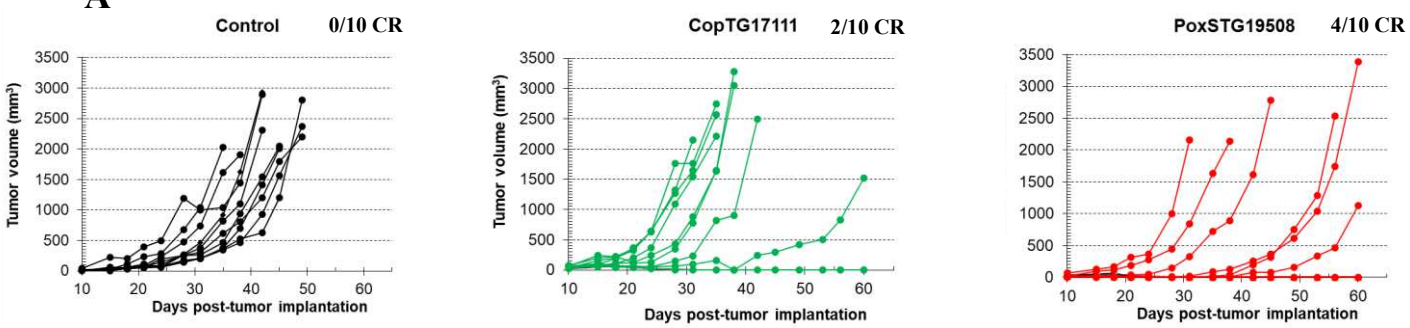


Figure 6. *In vivo* anti-tumor efficacy of PoxSTG in colorectal and hepatocarcinoma xenograft models. Subcutaneous xenografts were established in the right flank of nude mice using HCT116 colorectal cancer cells (**A,B**) or HepG2 hepatocarcinoma cells (**C,D**). Mice received a single intravenous injection of PBS (control), CopTG17111 or PoxSTG19508 at the indicated dose (vertical arrow). In the HCT116 model, treatment was administered on day 15 post-implantation at 3×10^4 PFU (n = 9 mice per group). In the HepG2 model, treatment was administered on day 28 post-implantation at 3×10^5 PFU (n = 10 mice per group). (**A,C**) Tumor volume progression for individual mice; inset tables summarize statistical comparisons between treatment groups. (**B,D**) Kaplan–Meier survival curves. Tumor volume data were analyzed using a mixed-effects model to account for repeated measurements over time. Survival differences were assessed using the log-rank test. Not significant (ns); $p < 0.05$ (*), $p < 0.0001$ (****). CR, complete response.

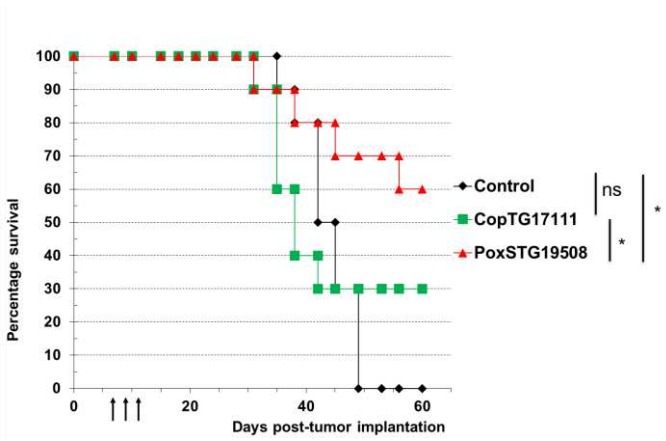
Figure 7

A

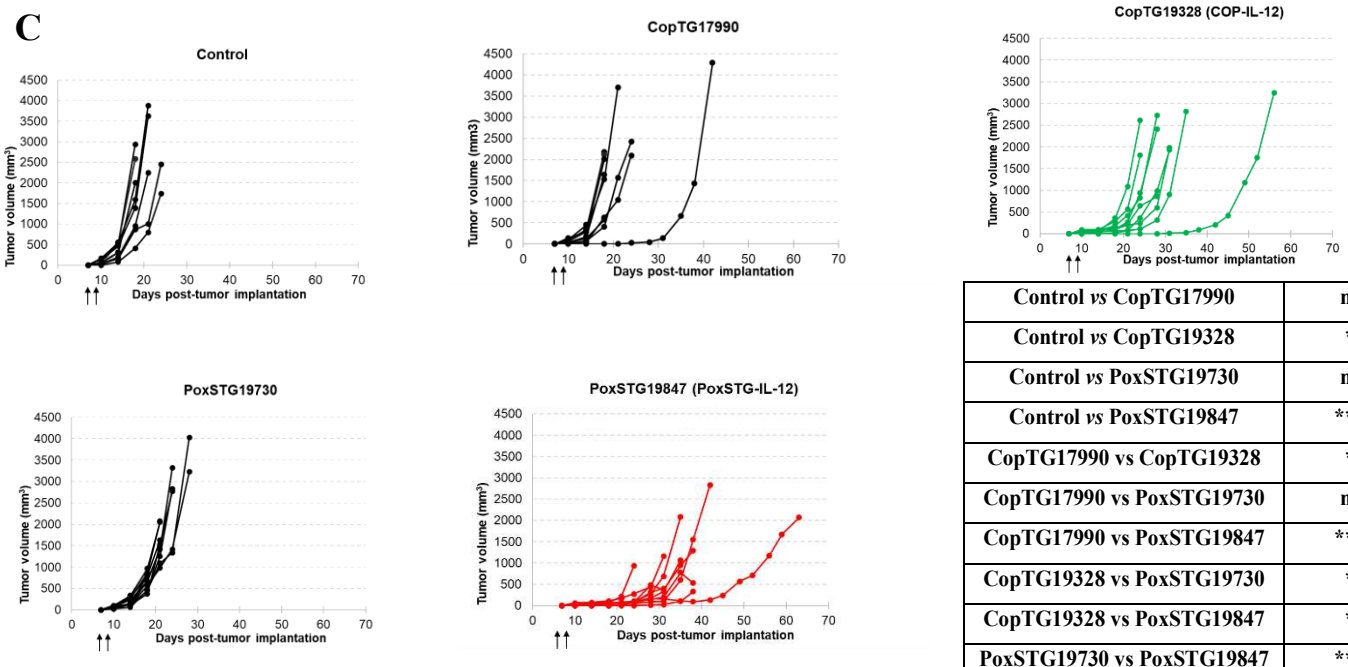


Control *vs* CopTG17111	ns
Control *vs* PoxSTG19508	**
CopTG17111 *vs* PoxSTG19508	**

B



C



Control *vs* CopTG17990	ns
Control *vs* CopTG19328	*
Control *vs* PoxSTG19730	ns
Control *vs* PoxSTG19847	***
CopTG17990 vs CopTG19328	*
CopTG17990 vs PoxSTG19730	ns
CopTG17990 vs PoxSTG19847	***
CopTG19328 vs PoxSTG19730	*
CopTG19328 vs PoxSTG19847	*
PoxSTG19730 vs PoxSTG19847	***

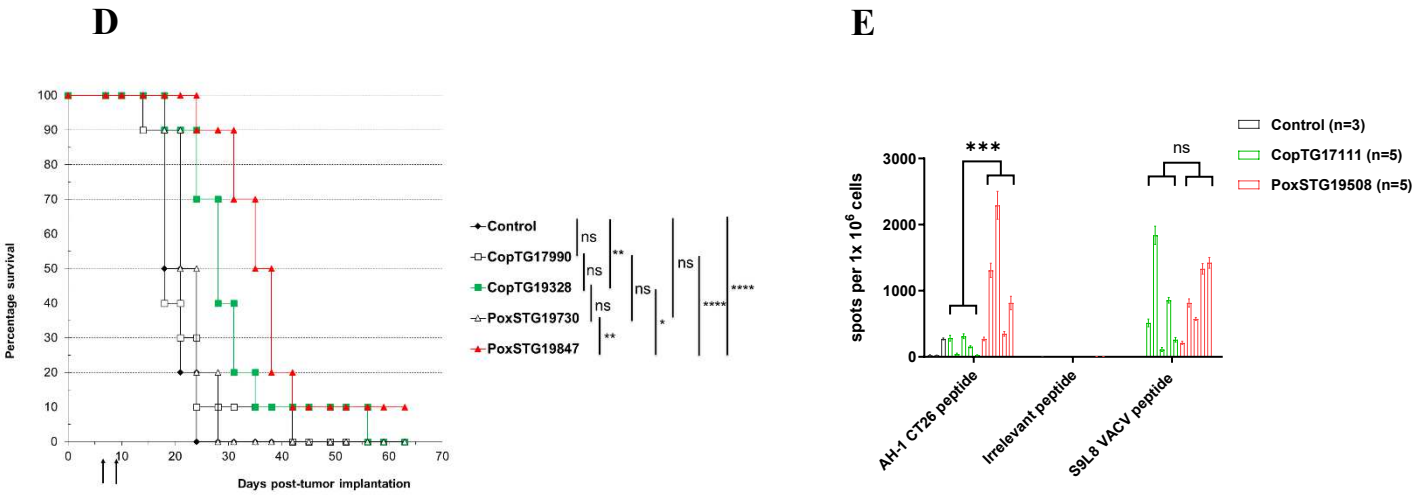
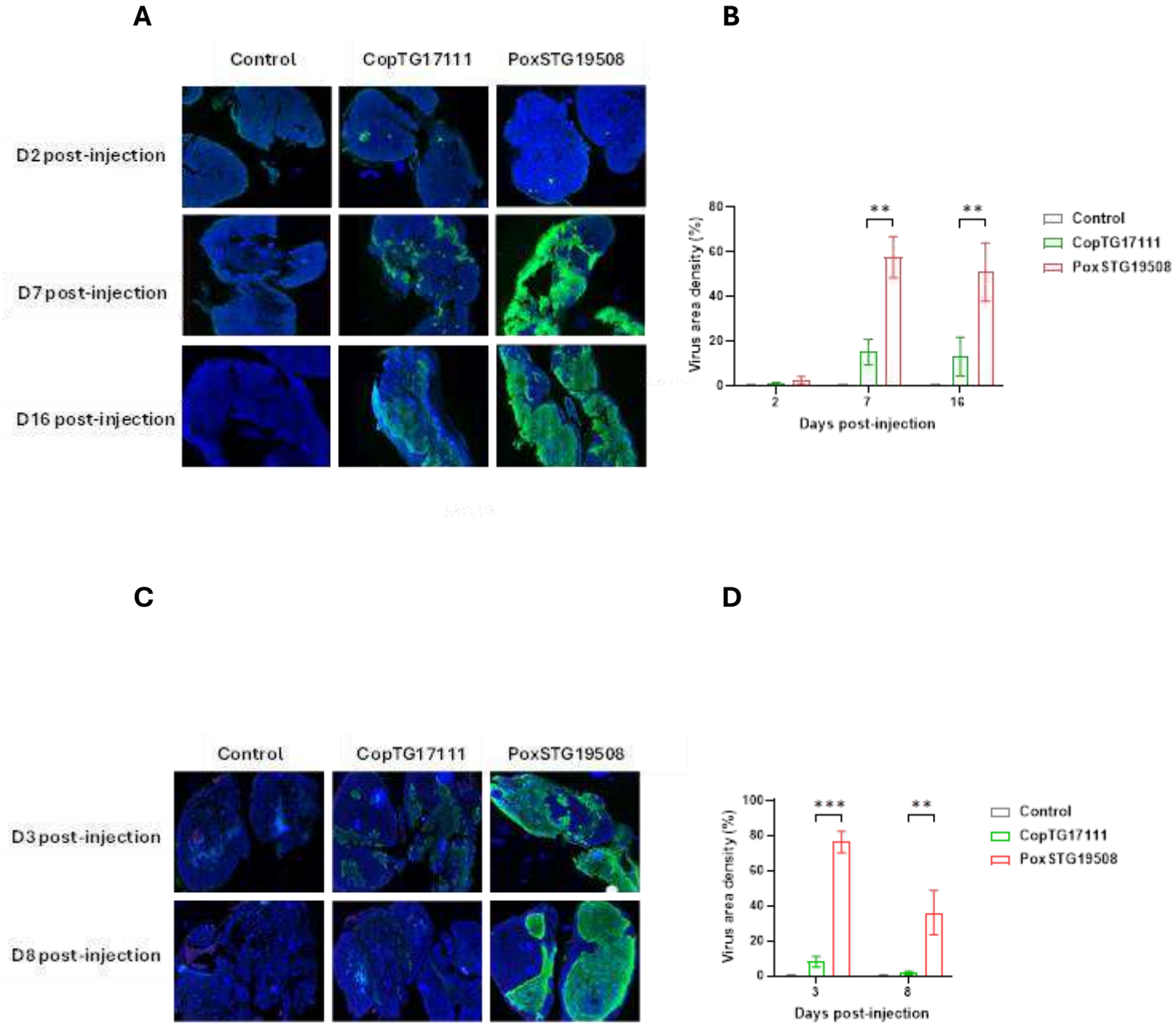
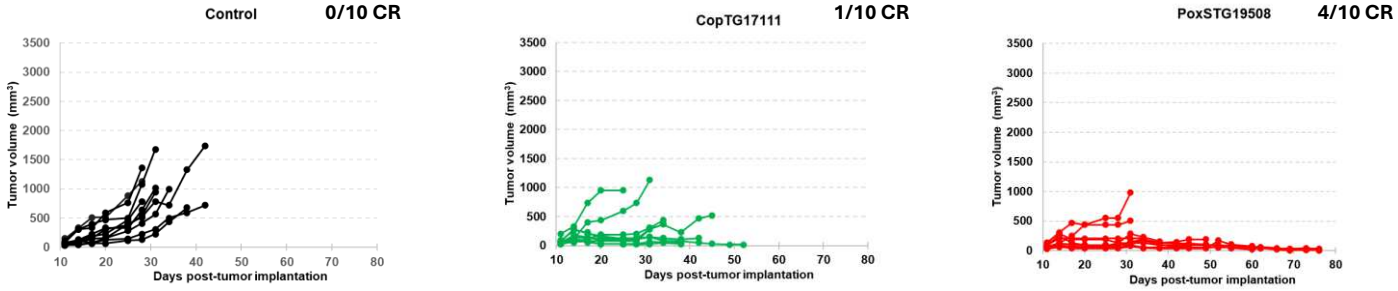


Figure 7. *In vivo* anti-tumor efficacy of PoxSTG in syngeneic murine tumor models and associated antigen-specific T cell responses. Antitumor activity of PoxSTG in CT26 (**A,B**) and of IL-12–encoding PoxSTG in B16F10 (**C,D**) syngeneic models. Mice received PBS (control) or the indicated viruses (arrows). In CT26 (**A,B**), mice were treated intratumorally with PBS (control), CopTG17111, or PoxSTG19508 at 1×10^7 PFU on days 7, 9, and 11 post-implantation (n = 10 mice per group). In B16F10 (**C,D**), mice received intravenous injections of PBS (control), CopTG17990, CopTG19328, PoxSTG19730, or PoxSTG19847 at 1×10^7 PFU on days 7 and 9 post-implantation (n = 10 mice per group). (**A,C**) Individual tumor volume curves; inset tables summarize statistical comparisons between treatment groups. (**B,D**) Kaplan–Meier survival. Tumor volume data were analysed using a mixed-effects model to account for repeated measurements over time. Survival differences were assessed using the log-rank test. (**E**) Antigen-specific T cell responses by IFN-γ ELISpot in splenocytes from CT26-bearing mice treated intratumorally with CopTG17111 or PoxSTG19508 (single dose, 1×10^7 PFU; n = 5/group). Responses to tumor (AH1 peptide) and viral antigen (S9L8 peptide) were evaluated after restimulation. An irrelevant peptide served as negative control. Data are presented as mean ± SEM of quadruplicate wells, expressed as the number of spots per 10^6 splenocytes. ELISpot statistical significance was determined by pairwise comparison using Tukey's adjustment. Not significant (ns); $p < 0.05$ (*), $p < 0.01$ (**), $p < 0.001$ (***), $p < 0.0001$ (****). CR, complete response.

Figure 8

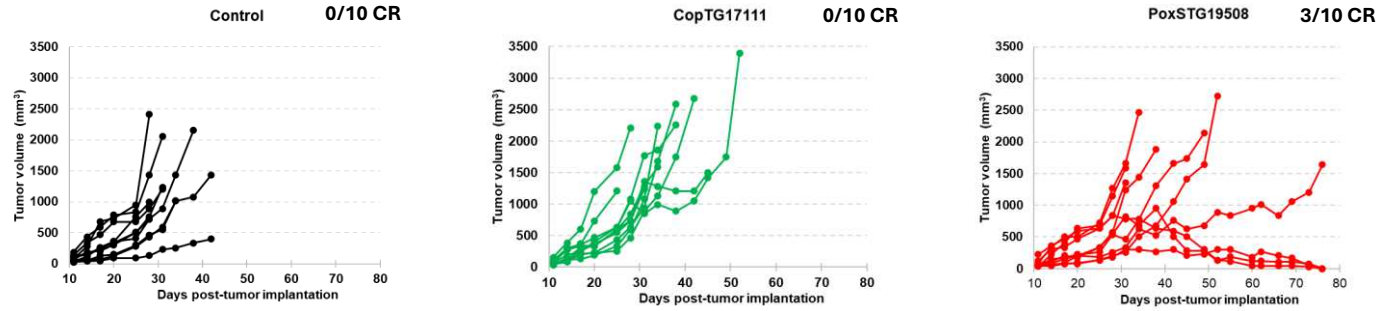

A
Control
CopTG17111
PoxSTG19508
D2 post-injection
D7 post-injection
D16 post-injection
B
Virus area density (%)
80
60
40
20
0
**
**
2
7
16
Days post-injection
Control
CopTG17111
PoxSTG19508
C
Control
CopTG17111
PoxSTG19508
D3 post-injection
D8 post-injection
D
Virus area density (%)
100
80
60
40
20
0
***
**
3
8
Days post-injection
Control
CopTG17111
PoxSTG19508

E



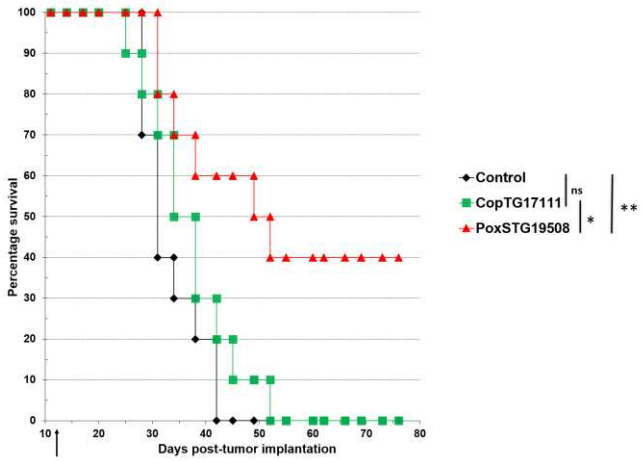
Control *vs* CopTG17111	********
Control *vs* PoxSTG19508	********
CopTG17111 *vs* PoxSTG19508	**ns**

F



Control *vs* CopTG17111	**ns**
Control *vs* PoxSTG19508	******
CopTG17111 *vs* PoxSTG19508	******

G



H

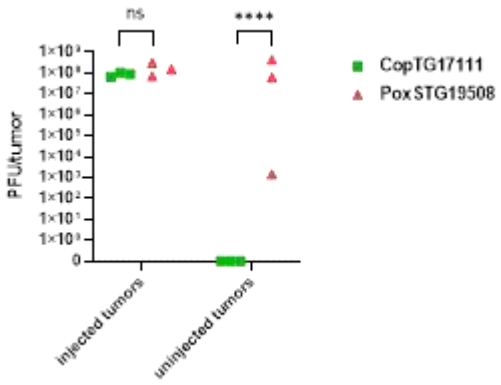


Figure 8. Enhanced intratumoral and systemic dissemination of PoxsTG.

(**A–D**) Viral spread in HCT116 xenograft and B16F10 syngeneic tumors. (**A**) Representative immunofluorescence images of HCT116 xenograft tumors collected 2, 7, and 16 days after a single intravenous administration of the indicated virus (1×10^5 PFU). Nuclei were stained with DAPI (blue), and viral infection was visualized in green. (**B**) Quantification of viral area density in HCT116 tumors shown in (A) (n = 3 tumors per group; mean ± SD). Statistical significance was assessed by one-way ANOVA; $p < 0.01$ (**). (**C**) Representative immunofluorescence images of B16F10 tumors collected 3 and 8 days after a single intratumoral injection of the indicated virus (1×10^7 PFU). (**D**) Quantification of viral area density in B16F10 tumors shown in (C) (n = 3 tumors per group; mean ± SD). Statistical significance was assessed by one-way ANOVA; $p < 0.01$ (**), $p < 0.001$ (***). (**E–H**) In vivo antitumor efficacy of PoxsTG19508 in a bilateral-flank xenograft model. Subcutaneous HCT116 tumors were established bilaterally, and only the right-side tumors were treated by intratumoral injection with CopTG17111, PoxsTG19508 (1×10^6 PFU), or PBS (control) (n = 10 mice per group). (**E**) Growth kinetics of injected tumors. (**F**) Growth kinetics of contralateral uninjected tumors. Insets summarize statistical comparisons between treatment groups. (**G**) Kaplan–Meier survival analysis. The arrow indicates the time of intratumoral virus administration. (**H**) Viral titers in injected and uninjected tumors 13 days after virus administration. Each dot represents an individual tumor. For longitudinal tumor-volume analyses, statistical significance was determined using a mixed-effects model. Survival differences were analyzed using the log-rank test. Viral titers (n = 3 tumors per group) were analyzed by one-way ANOVA. Not significant (ns), $p < 0.05$ (*), $p < 0.01$ (**), $p < 0.0001$ (****). CR, complete responses.

Supplementary Table 1

Code	Species	Strain	Accession No	Size of final assembled genome	Size of assembled ITR
COP	Vaccinia virus	Copenhagen	M35027	175,860	8,158
WR	Vaccinia virus	Western Reserve	AY243312	181,419	6,938
WY	Vaccinia virus	Wyeth	OP821762	182,664	16,306
MVA-GFP	Vaccinia virus	Modified Vaccinia Ankara expressing GFP	U94848	163,444	3,988
CPXV	Cowpox virus	Brighton	NC_003663	212,521	6,507
RCNV	Raccoonpox virus	Herman	NC 001989	201,260	1,737
RPXV	Rabbitpox virus	Utrecht	AY484669	186,491	3,462
ORFV	Orf virus	NZ2	DQ184476	133,176	2,032
PCPV	Pseudocowpox	TJS	KY463455	128,008	12,426
BPSV	Bovine Papular stomatitis virus	Illinois 721	None	133,871	863
MYXV	Myxoma virus	Lausanne	NC_001132	150,327	11,604
SQFV	Squirrelpox virus	Kilham	NC 022563	147,605	No ITR
FWPV	Fowlpox virus	FP9	NC_002188	248,557	6,500
SWPV	Swinepox virus	Kasza	None	122,765	3,597
YLDV	Yaba-like disease virus	Davis	NC 002642	142,724	1,915
CTV	Cotia virus	SP AN 32	NC 016924	158,746	939
PoxSTG	Chimeric poxvirus			185,577	9,667

Supplementary Table 1. Size of the *de novo* assembled genomes and ITR.

Virus short name and full names are indicated in the two first columns. Size of the mono-ITR genome and the assembled ITR only are reported in the 3rd and 4th column, respectively.

Supplementary Table 2

Viral Genes (VACV Copenhagen gene nomenclature)	Key function	Origines
A34R	Glycoprotein required for the infectivity of EEV	Chimeric gene: N-terminal portion from MVA and C-terminal portion from RPXV
A41L	Chemokine binding protein	RPXV
A46R	TLR inhibitor and putative IL-1 antagonist	RPXV
A48R	Thymidylate kinase	RPXV
A49L	Affects NF-kB and Wnt signaling cascades	RPXV
A52R	Putative inhibitor of TLR signaling	RPXV
A53R	Soluble TNF receptor	RPXV
A56R	Hemagglutinin	RPXV
B5R	Inhibits complement	WY
B8R	IFN-g soluble receptor	WY
B13R	Inhibits IL-1b converting enzyme	WY
B14	Inhibits NF-kB	WR
B15R	IL-1b soluble receptor	WR
B18R	IFN-a/b soluble receptor	WR
C3L (VCP)	Complement control protein	WR
C4L	Inhibits NF-kB	WY carrying a frameshift mutation leading to the loss of the last 64 C-terminal amino acids
C6L	Binds to STA2 and inhibits type I IFN signaling	WY
C7L	Antagonizes IRF-1 induced antiviral activities	WY
C12L	Binds and inhibits IL-18	WY
C21L	Complement control protein	WY
E3L	Binds dsRNA to block PKR activation	CPXV
F1L	Inhibits cytochrome C	CPXV
F4L	Ribonucleotide reductase small subunit	CPXV
I4L	Ribonucleotide reductase large subunit	RPXV
J2R	Thymidine kinase	WR
K1L	Inhibits NF-kB activation	CPXV
K3L	Inhibits dsRNA-activated protein kinase	CPXV
K7R	Promotes histone methylation associated with heterochromatin association	CPXV
M1L	Associates with apoptosome	CPXV
M2L	Inhibits NF-kB	CPXV
N1L	Inhibits NF-kB	CPXV
N2L	IRF3 inhibitor	CPXV

Supplementary Table 2. List of PoxSTG genes, their functional roles, and their origins.

The table presents a list of selected genes incorporated into the PoxSTG platform, along with their respective biological functions and natural origins. Virus abbreviations: CPXV (Cowpox virus), MVA (Modified Vaccinia Ankara), RPXV (Rabbitpox virus), WR (Vaccinia virus Western Reserve strain), WY (Vaccinia virus Wyeth strain).